THE GEOLOGICAL SOCIETY OF AMERICA®

Debris flow initiation from ravel-filled channel bed failure following wildfire in a bedrock landscape with limited sediment supply

Marisa C. Palucis[1,†], Thomas P. Ulizio[2], and Michael P. Lamb[2]
[1]*Department of Earth Sciences, Dartmouth College, 6105 Fairchild Hall, Hanover, New Hampshire 03755, USA*
[2]*Division of Geological and Planetary Sciences, California Institute of Technology, 1200 E California, Boulevard, Pasadena, California 91125, USA*

ABSTRACT

Steep, rocky landscapes often produce large sediment yields and debris flows following wildfire. Debris flows can initiate from landsliding or rilling in soil-mantled portions of the landscape, but there have been few direct observations of debris flow initiation in steep, rocky portions of the landscape that lack a thick, continuous soil mantle. We monitored a steep, first-order catchment that burned in the San Gabriel Mountains, California, USA. Following fire, but prior to rainfall, much of the hillslope soil mantle was removed by dry ravel, exposing bedrock and depositing ~0.5 m of sandy sediment in the channel network. During a one-year recurrence rainstorm, debris flows initiated in the channel network, evacuating the accumulated dry ravel and underlying cobble bed, and scouring the channel to bedrock. The channel abuts a plowed terrace, which allowed a complete sediment budget, confirming that ~95% of sediment deposited in a debris flow fan matched that evacuated from the channel, with a minor rainfall-driven hillslope contribution. Subsequent larger storms produced debris flows in higher-order channels but not in the first-order channel because of a sediment supply limitation. These observations are consistent with a model for post-fire ravel routing in steep, rocky landscapes where sediment was sourced by incineration of vegetation dams—following ~30 years of hillslope soil production since the last fire—and transported downslope by dry processes, leading to a hillslope sediment-supply limitation and infilling of low-order channels with relatively fine sediment. Our observations of debris flow initiation are consistent with failure of the channel bed alluvium due to grain size reduction from dry ravel deposits that allowed high Shields numbers and mass failure even for moderate intensity rainstorms.

INTRODUCTION

Understanding sediment transport processes on steep slopes is important, especially in regions prone to wildfire-flood cycles, such as rapidly eroding regions of the American southwest (Kotok and Kraebel, 1935; Wells et al., 1987; Singleton et al., 2019). For example, many steep basins (e.g., average hillslope angles greater than ~30°) within the San Gabriel Mountains, California, USA, lack a thick, continuous soil mantle (i.e., hillslopes that have a thick soil cover and relatively little bedrock outcropping [Dietrich et al., 1986]) and instead have patches of bare bedrock, talus, and thin soil cover (DiBiase et al., 2010; Heimsath et al., 2012), where local slope stability is often provided by vegetation (Lamb et al., 2011, 2013; DiBiase and Lamb, 2013). DiBiase and Lamb (2020) showed that—due to spatial heterogeneity in soil-mantled and bedrock-dominated hillslopes within the San Gabriel Mountains—sediment response after fires can vary greatly even on neighboring hillsides. Because post-fire sediment yield can greatly exceed background rates (Moody et al., 2013), it is important from a hazard mitigation perspective to understand how sediment is delivered from soil-mantled and bedrock-dominated hillslopes to the channel (e.g., Roering and Gerber, 2005; Lamb et al., 2011; DiBiase and Lamb, 2020) as well as how sediment moves from lower to higher order channels (i.e., via flooding or debris flows). In many post-fire landscapes, debris flow occurrence has been observed to increase (Hyde et al., 2007; Gartner et al., 2008; Cannon et al., 2011; Riley et al., 2013), while at the same time fire suppression practices and drought are increasing the frequency, intensity, and extent of wildfires in these same regions (Miller et al., 2009; Marlon et al., 2012; Dennison et al., 2014). Understanding the connection between wildfire, sediment yield, and debris flow occurrence is increasingly important for hazard mitigation (Santi et al., 2008; Lin et al., 2012).

Debris flows can initiate though a number of mechanisms that can occur either on the hillslope or in the channel. On hillslopes, landslides can be triggered during rainstorms due to increased soil pore pressures, often in thick and vegetated colluvium, before being mobilized into debris flows within the channel network (Iverson et al., 1997; Gabet and Mudd, 2006). Sediment entrainment by surface runoff on the hillslope can also cause debris flows via systems of coalescing rills (Meyer and Wells, 1997; Cannon et al., 2001a; Godt and Coe, 2007; Kean et al., 2011). After wildfires, the role of overland flow is potentially enhanced due to the loss of vegetation and changes in soil properties, such as increased hydrophobicity and decreased permeability (e.g., Gabet and Sternberg, 2008; Parise and Cannon, 2012). Concentrated runoff can lead to thin debris flows, such as shallow, ~1–3-cm-thick failures of the soil surface (Gabet and Sternberg, 2008; Langhans et al., 2017) as well as progressive entrainment of material that transforms into debris flows (Meyer and Wells, 1997; Gabet and Bookter, 2008). As surface vegetation and root strength recover, which can take as long as decades after a severe fire, the occurrence of sediment-entraining runoff (e.g., Inbar et al., 1998), dry ravel (e.g., Mersereau and Dyrness, 1972; Megahan et al., 1995), and shallow debris slides (Wondzell and King, 2003) can decline. However, due to the loss of deep root strength from trees, deep-seated landslides can increase (Swanson, 1981; Cannon et al., 2001b). Therefore, sediment yield often increases immediately following fire, and slightly elevated rates can persist for decades (Benda and Dunne, 1987; Cerdà and Doerr, 2005). Given an inexhaustible supply of hillslope soil, increased fire frequency

Marisa Palucis http://orcid.org/0000-0003-0034-5810
[†]marisa.c.palucis@dartmouth.edu.

 https://doi.org/10.1130/B35822.1; 14 figures; 1 table.

may lead to increased sediment yields, greater debris flow hazards, and long-term changes in landscape morphology (e.g., Roering and Gerber, 2005; Jackson and Roering, 2009).

While debris flows triggered from landsliding and hillslope soil erosion may dominate on portions of the landscape that have thick soil mantles, in steeper regions, post-fire debris flows may be triggered in channels instead (e.g., McGuire et al., 2017), and hillslope sediment can be supply limited (Lamb et al., 2011). In these very steep portions of the landscape, soils are often patchy and gravitationally unstable, and transient sediment storage on the hillslope, where it occurs, is enabled by vegetation (DiBiase and Lamb, 2013). During wildfire, vegetation dams are incinerated, which can rapidly release a large volume of sediment to river channels though dry ravel (the rolling, bouncing, and sliding of particles downhill without fluid) (e.g., Florsheim et al., 1991; Gabet, 2003; Jackson and Roering, 2009; Lamb et al., 2011). This process can erode hillslope soil and load channels with relatively fine-grained sediment prior to rainfall (DiBiase and Lamb, 2020). Channel bed fining can increase Shields numbers by orders of magnitude, even for moderate storm events, making failure of the alluvial channel bed more likely (Prancevic et al., 2014; Palucis et al., 2018). For debris flows derived from channel bed failure, the frequency and size of the flows are dictated by transient storage and release of sediment by vegetation dams. Therefore, increasing fire frequency due to a warming climate may not result in increased hazard due to sediment supply limitations (Lamb et al., 2011).

Mechanisms for in-channel debris flow initiation include collapsing channel banks or dams that lead to the transformation of clear water flow into debris flows (Takahashi, 1978; Berti et al., 1999), channel morphology or spatial variability in flow (e.g., jets and pools) that can induce rapid sediment entrainment and failure (Costa, 1984; Berti et al., 1999; Cannon et al., 2003; Kean et al., 2013), progressive fluvial entrainment and bulking (Gabet and Bookter, 2008), and failure of the alluvial channel bed itself due to seepage and overland flow (Takahashi, 1978; Prancevic et al., 2014). For channel bed slope angles (S) less than $\sim$2°, sediment is typically transported fluvially (Stock and Dietrich, 2003), but Prancevic et al. (2014) and Prancevic et al. (2018)—who recast the Takahashi (1978) model in terms of a critical Shields stress for debris flows—showed through flume experiments that there exists a threshold slope, S_c, above which mass failure of the channel bed occurs prior to any fluvial grain entrainment (S_c $\sim$22°). Palucis et al. (2018) showed experimentally that for moderate channel slopes (i.e., $5° < S < 17°$) under high Shield stresses, dense, granular sheetflows occur. This is a transitional transport process between dilute river transport and debris flows. Particle jamming at boulder steps (Kean et al., 2013) and waterfalls (Johnson and Rodine, 1984; Godt and Coe, 2007) can also be important in triggering debris flows in channels. The latter is often termed "the fire-hose effect" (Johnson and Rodine, 1984), in which a plunging jet fluidizes a sediment bed (e.g., Scheingross and Lamb, 2016).

Due to the variety of possible debris flow initiation mechanisms, the steep terrain on which they initiate, and their sporadic nature, there is only a limited set of direct observations of where (e.g., Kean et al., 2013; Staley et al., 2014) and under what rainfall conditions (e.g., Staley et al., 2017; Tang et al., 2019a) debris flows initiate, and many of these observations are of unburned catchments (e.g., Berti et al., 2000; McArdell et al., 2007; Suwa et al., 2009; McCoy et al., 2010). Most direct observations of debris flows are in higher order channels or downstream from where debris flows initiated, which reveal debris flow occurrence but do not directly reveal debris flow initiation sites—whether on hillsides or in low-order channels (e.g., Marchi et al., 2002; Hürlimann et al., 2003; McCoy et al., 2010; Suwa et al., 2011).

Because of limited observations of debris flow initiation and a lack of simple mechanistic models for predicting where on a landscape debris flows will initiate (e.g., Kean et al., 2013; McGuire et al., 2016, 2017), the standard forecasting method is to use empirical rainfall intensity duration thresholds (Guzzetti et al., 2008; Baum and Godt, 2010; Cannon et al., 2011), taking into account parameters such as catchment topography and area, burn severity, soil properties, and sediment supply (Cannon et al., 2010; Staley et al., 2017). Burn severity and hillslope soil properties are likely more important for predicting mass failure on soil-mantled hillslopes, where changes in soil hydrophobicity and permeability can promote runoff and rilling (e.g., Wells, 1987; Spittler, 1995; Wondzell and King, 2003). In catchments that are dominated by bedrock outcrops (i.e., >50% of the basin has thin to no soil cover, often with average local slopes greater than $\sim$30° [e.g., DiBiase, 2011]), dry ravel, and failure of channel fills, the importance of these factors is less clear. So, while these empirical models are useful and necessary, more mechanistic models are needed that incorporate the hydrologic and geomorphic processes that control sediment production, transport, and storage at the initiation site.

To investigate post-fire debris flows in a bedrock-dominated landscape and evaluate hillslope versus in-channel initiation mechanisms, we monitored a first-order, steep, and recently burned catchment within the front range of the San Gabriel Mountains, California, immediately following wildfire and over the course of several subsequent winter storms. We used topographic analysis from unmanned aerial vehicle (UAV) photography, water and sediment routing models, and field observations to accomplish the following major objectives: (1) compare modeled ravel routing to field observations, (2) perform a catchment-wide mass balance for sediment moved by storm events following fire, and (3) use a simple rainfall runoff model to predict where in-channel debris flows would occur and compare its results to our field observations.

FIELD SETTING AND PREVIOUS WORK

The San Gabriel Mountains are tectonically active and result from a restraining bend in the San Andreas fault, where active thrusting along the Sierra Madre and Cucamonga fault zones maintained Holocene vertical slip rates of 0.5–0.9 mm/yr (e.g., Lindvall and Rubin, 2007), and uplift began at ca. 5–7 Ma with a change in activity from the San Gabriel fault to the current trace of the San Andreas fault (Matti and Morton, 1993). Exhumation and cosmogenic radionuclide exposure ages indicate erosion rates on the order of $\sim$0.5 mm/yr (Spotila et al., 2002; Lavé and Burbank, 2004; DiBiase et al., 2010). Along-slip variations in the range led to west-east gradients in hillslope angle, topographic relief, and channel steepness (DiBiase et al., 2010). The landscape is steep, with 60–80% of the landscape exceeding 30° slopes (Lamb et al., 2011). Rock exposure is patchy, and intermittent soil cover persists throughout the range despite hillslope angles above the angle of repose (DiBiase et al., 2010). The geology of the San Gabriel Mountains is mainly Precambrian crystalline basement rock and Mesozoic granitic intrusions (Morton et al., 2006).

The San Gabriel Mountains are an ideal natural laboratory for studying the connection between wildfire and sediment transport processes. They have been studied intensively for nearly a century; destructive debris flows on 1 January 1934 were documented following a fire in November that affected the Los Angeles basin towns of Montrose and La Crescenta (Eaton, 1935). Given the hazards associated with debris flows and the San Gabriel Mountains' close proximity to urban centers, Los Angeles County has captured sediment exiting over 150 catchments into debris basins since the 1920s, providing one of the longest records of sediment fluxes from steep, fire-prone terrain (Rowe et al., 1954; LACDPW, 1991; Lavé and

Burbank, 2004; Lamb et al., 2011). Early studies on post-fire erosion and mitigation by the U.S. Forest Service focused on the lower gradient portions of the San Gabriel Mountains, within the San Dimas Experimental Forest, where field observations led to the conceptual model that debris flow initiation in the region was due to hillslope failures resulting from the loss of stabilizing vegetation and increased soil hydrophobicity (e.g., Anderson, 1949; Sinclair, 1954; Wells, 1982; Dunn et al., 1988). However, there are relatively few direct observations of debris flows in the steeper, bedrock-dominated portion of the mountain range, which dominates the majority of the terrain and also produces the most significant response in increased wildfire sediment yields (e.g., Cannon et al., 2008; Lamb et al., 2011; Gartner et al., 2014).

Recent efforts by the U.S. Geological Survey have documented debris flow occurrences within burned catchments typically near catchment mouths (e.g., Kean et al., 2011; Tang et al., 2019b, 2019a), and others have analyzed historic debris basin data for trends among sedimentation rates and wildfire occurrence (e.g., Lamb et al., 2011; DiBiase and Lamb, 2013; Gartner et al., 2014). Several studies have used repeat terrestrial laser scanning to document hillslope transport processes, which revealed moderate rilling and ravel production on hillslopes (e.g., Schmidt et al., 2011; Staley et al., 2014), but they have tended to focus on hillslopes below the threshold slope for dry ravel that maintain a semi-stable soil mantle after fire and did not document debris flow initiation. DiBiase and Lamb (2020) used repeat airborne lidar to reveal widespread loading of low-order channels following wildfire and prior to rainfall. Direct observations of debris flow initiation zones in low order channels are rare (Tillery and Rengers, 2020); therefore, it remains unclear whether sediment supply limits debris flow occurrence (e.g., Kean et al., 2011, 2013; Lamb et al., 2011, 2013; McGuire et al., 2017; Tang et al., 2019b) and if ravel-filled channels are debris flow initiation sites (e.g., Florsheim et al., 1991; Kean et al., 2011; Lamb et al., 2011; DiBiase et al., 2017). To address this knowledge gap, we chose to monitor a steep, burned, first-order catchment that we hypothesized could be a debris flow initiation site.

Our selected field site was near the mouth of Van Tassel Canyon (34.1566°N, 117.93528°W) (Fig. 1), located in the southern San Gabriel Mountains to the northeast of Los Angeles.

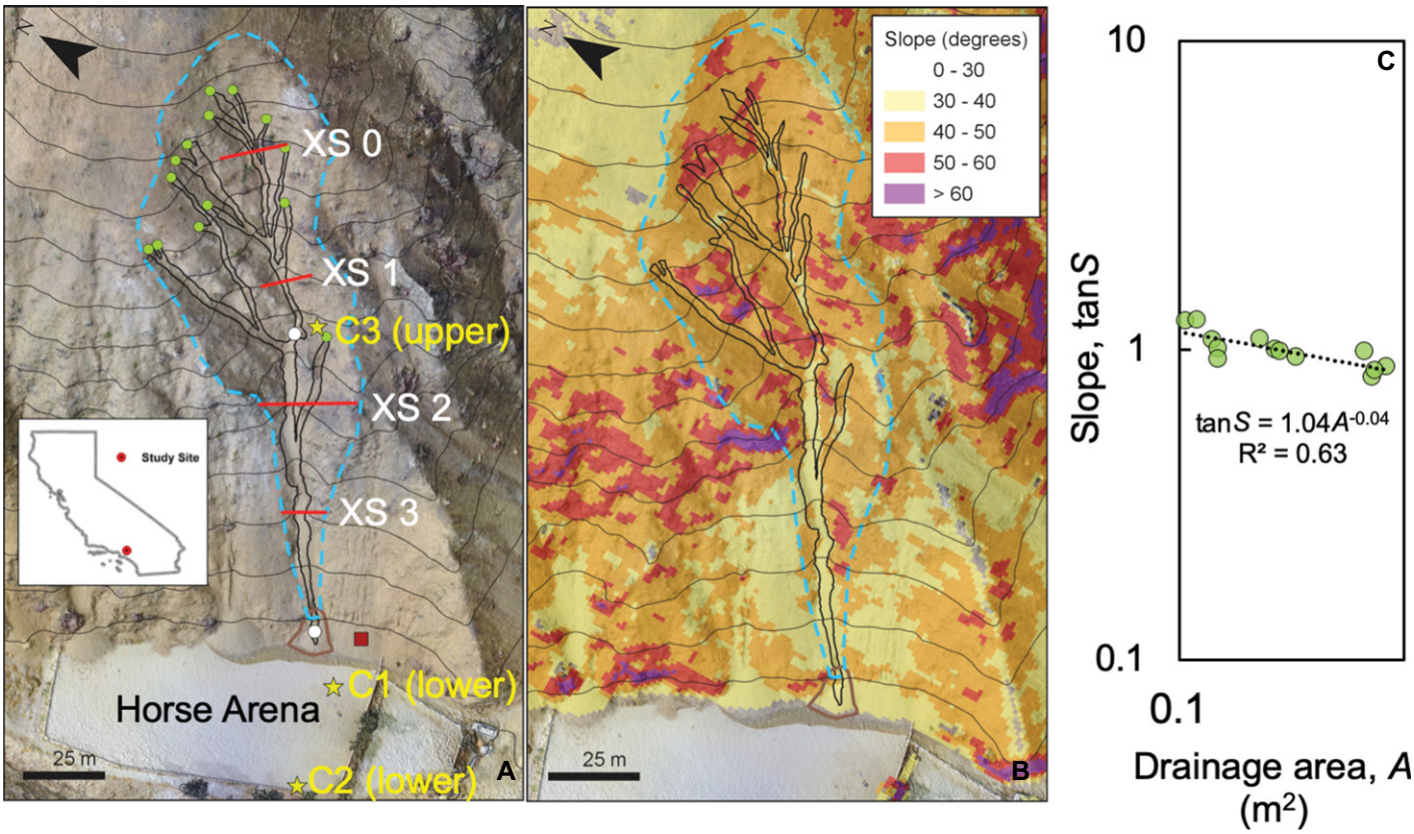

Figure 1. (A) Downward-looking aerial image shows the study site (catchment area ~6600 m^2), which is located on a hillside adjacent to the northernmost training arena at the Encanto Equestrian Center in Duarte, California. The three process domains, the channel network (outlined in black), the hillslope (outlined with blue dashes and not including the channel network), and the depositional domain (ravel cone outlined in brown) are mapped. We installed three time-lapse cameras (yellow stars), two in the depositional zone (labeled C1 and C2) and one near a bedrock knickpoint (C3). Ravel depth measurements (white circles) and a ravel sample (red square) for grain size measurements were made on 27 October 2016, following the Fish Fire but prior to a rain event. Channel heads are indicated by green circles, and the locations of channel cross-sections (Fig. 11) are shown in red. Light black lines are topographic contours with a contour interval of 10 m. The inset shows the location of the field site within California, USA. (B) Slopeshade of study site, where slope values were generated from our reference digital elevation model (e.g., Survey 1) based on the steepest local slope of each pixel and smoothed with a 10 m moving window. (C) The tangent of the bed slope angle (tan*S*) plotted as a function of drainage area (*A*, in m^2) in log-log space for channel heads, whose locations are marked with green circles in (A).

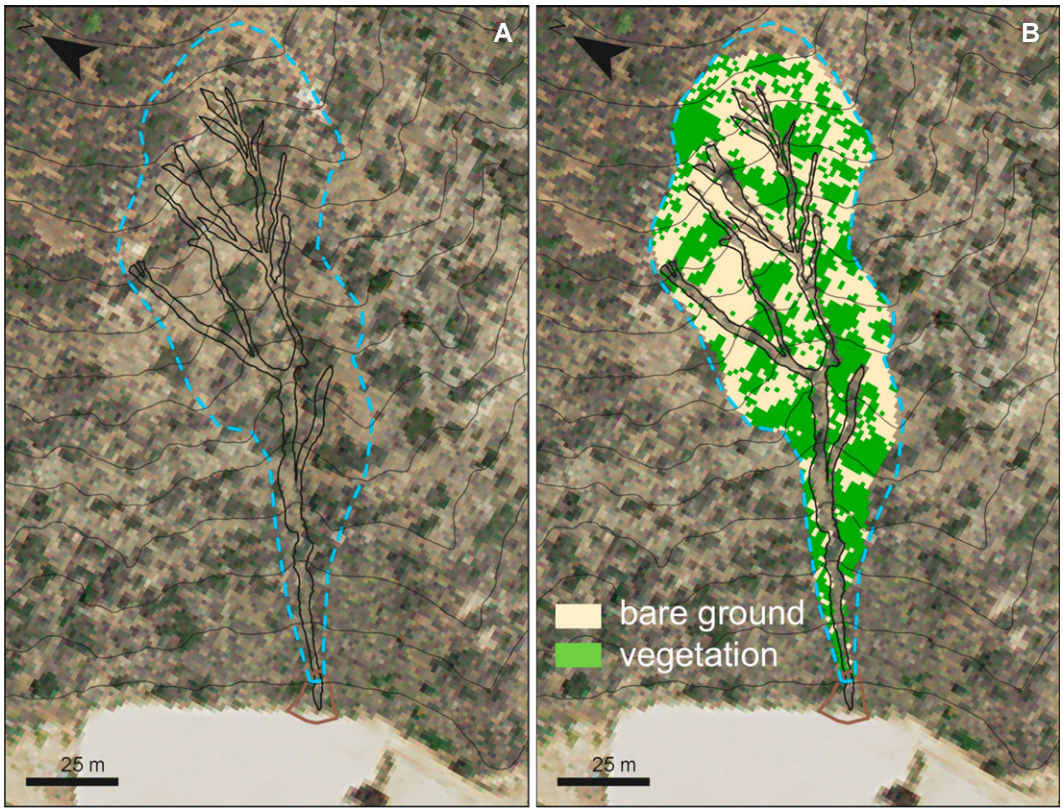

Figure 2. (A) National Agriculture Imagery Program (NAIP) orthorectified multispectral image over the study site was acquired on 2 June 2016 (m_3411856_nw_11_h_20160602, 0.6 m per pixel resolution). (B) Image from (A) rendered as a Normalized Difference Vegetation Index (NDVI) within the study catchment using the red (RED, 619–651 nm) and near-infrared (NIR, 808–882 nm) bands, where NDVI, (RED – NIR) / (RED + NIR), can vary between −1 and 1. All NDVI values between −1 and 0.5 were classified as bare ground, and all values between 0.5 and 1 were classified as vegetation (i.e., woody chaparral).

The site was chosen because it was steep, had recently burned, was easily accessible, the channel was visibly filled with ravel, and the hillslope abuts a terrace (which was cleared to make a horse arena). This terrace was important, as it provided a complete sediment trap, allowing for a catchment-wide mass balance. The site elevation ranges from ~245 m at the horse arena to ~400 m at the ridge top. The catchment area is ~6600 m^2 and has a mean slope angle of 44° ± 6° and a median of 44°. After the fire but prior to any rainfall, using drone imagery and field-truthing, we mapped ~56% of the catchment as being bare-bedrock or bedrock with a thin cover of soil (less than a few centimeters). Bedrock was typically observed where local slopes were >43°, which closely matched the observation by DiBiase (2011), who found excellent agreement between percent local slopes >45° and percent exposed rock in nearby terrain. Portions of the catchment that retained a sediment cover were near the northernmost ridge of the catchment as well as in the lower elevations of catchment (below XS 3, Fig. 1A). The site is part of a larger watershed that drains to the Las Lomas debris basin. The site burned in the 2016 Fish Fire (later called the San Gabriel Complex Fire) from 20 June 2016 to 23 July 2016, and ~21.8 km^2 burned in total. Before that, the site burned in the 1980 Stable Fire (~24.5 km^2 burned). The burn severity for the most recent fire at our site was mapped as low (The State of California and the Department of Forestry and Fire Protection, 2018), which is defined as scorched to charred litter, intact duff, partly consumed to charred woody debris, and black ash (Parson et al., 2010). The bedrock is quartz diorite (Morton, 1973). Vegetation within the catchment is normally composed of hard chaparral species, dominated by chamise, mountain mahogany, manzanita, and yucca, with pre-fire plant densities in nearby terrain of ~0.4 to ~0.5 plants/m^2 (Fig. 2) (Keeley, 1992).

Climate varies some across the San Gabriel range, with mean annual precipitation (MAP) of ~500 mm/yr over the Los Angeles basin to 1000 mm/yr along the ridge crest and back to 200 mm/yr in the rain shadow to the north. The MAP over the study site is ~620 mm/yr (www.prism.oregonstate.edu). Most precipitation in the southern San Gabriel Mountains is delivered by convective storms in the winter months. Streamflow was historically well-monitored in the region, but presently there are only two active U.S. Geological Survey (USGS) gages. Daily mean discharges scale with drainage area in the region, with mean annual runoff of ~280 mm/yr (or 30% of average rainfall) (DiBiase and Whipple, 2011). The average sediment yield, based on 93 nearby debris basins, is ~0.1–1 mm/yr (Lamb et al., 2011).

METHODOLOGY

Field Surveys and Measurements

To capture high-resolution topography, we conducted UAV surveys (DJI Phantom 4) post-fire, pre-storm (Survey 1, 27 October 2016), and then five days after the first major storm in the region (Survey 2, 21 December 2016). Subsequent drone scans were conducted during January 2017, which were used for a qualitative assessment of how the system evolved throughout the rainy season. The onboard RBG camera was 12.4 megapixels with a 24 mm lens. We also installed three time-lapse cameras (Moultrie M880) (yellow stars, Fig. 1A), two in the depositional zone (C1 and C2) and one at a small, ~1-m-high bedrock knickpoint in the channel (C3). Image resolution was 8 megapixels with a fixed camera focal length of 50 mm. Prior to each storm event, the cameras were set to take one image every 30 s; each image had a time-stamp (local time, hour:min) so images between cameras could be compared within ± 1 min. Laboratory tests did not show measurable time drift over 72 h, which is the longest they were deployed before being reset. We measured the depth of the ravel cone at its apex post-fire and pre-rainfall at five locations as well as the thickness of the ravel infill using rebar at three locations near the bedrock knickpoint, which was

located ~10 m upslope from the apex of the ravel cone (white circles, Fig. 1A). Reported ravel thicknesses are the mean ± standard deviation of measurements from these three sites. Sediment samples (~0.6–6 kg) were collected in a neighboring ravel cone (red square, Fig. 1A), the post-storm depositional fan lobes, and within post-storm debris flow levees for grain size analysis, where grain size fractions were measured by mechanical sieves (with 64 mm, 32 mm, 16 mm, 8 mm, 4 mm, 2 mm, and 1 mm sieves). Tilt table experiments were conducted on the pre-event ravel cone material using the median grain sizes (material sieved between 2 mm and 4 mm), following the methodology in Prancevic et al. (2014), to estimate failure plane friction angles, ϕ_f, which ranged from 36° to 47°.

Local precipitation data were provided by the USGS (Jason Kean, personal commun., 2017) at their monitoring site located ~125 m upstream from our field site (Tang et al., 2019b), which used a similar instrument as described in McCoy et al. (2010) and Kean et al. (2011). The measurements spanned from 11 December 2016, when the station was installed, to 24 January 2017. Given the small distance between our site and the USGS gage, we assumed negligible rainfall differences between the two locations. However, the rainfall data lagged several minutes behind observations made with our field cameras as the storm moved from south to north.

UAV-Derived Elevation Models

Three-dimensional point clouds were generated from structure-from-motion techniques using the commercially available Agisoft Photoscan software. Survey 1 was used as a reference survey, and Survey 2 was georeferenced to Survey 1. Our ground control points were mostly located on the horse arena at the base of the catchment, where x, y, z data were collected using a Septentrio RTK Altus NR3 with a horizontal accuracy of 0.6 cm and a vertical accuracy of 1 cm. Due to the steep nature of the site, and difficulty in collecting ground control points across the entire catchment, we manually identified 75 additional control points (i.e., locations that did not move between the two surveys, such as large boulders, bedrock outcrops, and distinct features on ridges) that spanned a range of elevations and aspects across the landscape. Points were mapped onto aerial images from Survey 1, and Photoscan was used to automatically identify each point in the remaining images. We then manually went through every image to ensure that all points were in the correct location, and if not, manually corrected them. This process was repeated for Survey 2 using the same 75 locations. For each ground control point, the x, y, z location was imported into Photoscan using a NAD 83 UTM zone 11N coordinate system and WGS84 projection system. Dense point clouds were generated for each survey in Photoscan before each cloud was imported into CloudCompare, which is an open source software. Further rectification was performed using the Statistical Outlier Filter algorithm to remove anomalous points and the Iterative Closest Point (ICP) algorithm to best align Survey 2 with Survey 1. Individual point cloud surveys were then converted to digital elevation models (DEM) with a rectangular grid at 25 cm/pixel resolution. The two surveys were differenced to calculate vertical erosion and deposition in the z-direction. Error in aligning the DEMs was quantified by calculating the difference between x, y, z values at each of our control points, which should be zero (i.e.,

$$\sqrt{(x_{pre}-x_{post})^2+(y_{pre}-y_{post})^2+(z_{pre}-z_{post})^2}\,),$$

and then taking the average of those differences. Due to the steep terrain, vertical errors can be large, as horizontal errors ($\delta \sim \sqrt{(x_{pre}-x_{post})^2+(y_{pre}-y_{post})^2}$ can translate into vertical errors of $\sim\delta S$, where S is the slope gradient (Pelletier and Orem, 2014). Errors in δ were <0.1 cm for all control points, such that almost all of the total error is due to error in the z (vertical) direction. The mean total error was −3.3 cm with a standard deviation of ±17 cm. Therefore, we considered any local difference measurement that was within the mean ± standard deviation of the control points (i.e., deposition < 20 cm; erosion > −14 cm) to be within error of zero elevation change, and they were excluded from our mass balance calculations.

Process Domains and Sediment Budget

Process domains within the catchment (blue dashed line, Fig. 1A) were mapped as hillslope, channel, and fan. We mapped out the hillslope and channel visually using imagery and topography, where the channel was defined as a region of topographic convergence that was concave-up in cross-section and formed a branching network (channel delineated by black line, Fig. 1A). The channel is small but differs from rills in that rills are ephemeral in soil, and the channel is a permanent feature in bedrock. Channel heads are often delineated from hillslopes in slope area space (Montgomery and Dietrich, 1989), and our mapped channel heads occur at bed slope angles of ~40°–50° (Figs. 1A–1B), where the data best fit a power-law relationship with drainage area (A, m^2) versus the tangent of the bed slope angle (tan$S$) (i.e., $\tan S = 1.04A^{-0.04}$) (Fig. 1C). The sediment yield from the first storm was completely captured within an alluvial fan that formed on the terrace at the base of the channel. The entire fan was due to post-fire sedimentation, as the terrace was plowed horizontal as a horse arena prior to the fire (Fig. 1A).

Erosion and deposition amounts were calculated by differencing the topographic surveys for each of the process domains (Fig. 3). Volumetric changes on the hillslope, channel, and fan were computed by summing the elevation differences within the domain boundaries and multiplying by the pixel area, and then were converted to mass using a dry bulk density of 1.44 g/cm^3 for the channel fill (based on samples collected prior to the first rainfall event) and 1.76 g/cm^3 for the fan deposit (based on samples collected after the first rainfall event). Bulk densities pre- and post-storm were determined by collecting a known volume (~1 L) of sediment in the field and weighing it after drying.

Sediment and Water Flow Routing

A 2-D particle-based, ravel routing model (DiBiase et al., 2017) was used to predict where ravel would accumulate within the catchment post-fire. The model extends purely probabilistic treatments of hillslope diffusion processes (Tucker and Bradley, 2010) by using a sliding block model (Gabet and Mendoza, 2012) to track the acceleration and deceleration of particles as they move downslope, explicitly accounting for hillslope topography, grain size, and surface roughness. The model uses a modified Coulomb friction law for the downslope acceleration of a particle (A_c)

$$A_c = g(\sin\theta - \tan\phi\cos\theta) - k\|V\|^a, \qquad (1)$$

and treats the effective (dynamic) friction angle between the particle and the hillslope, ϕ, as a stochastic variable due to the interaction of the grain with random roughness elements on the hillslope

$$\text{(i.e., } \tan\phi = \text{pdf}(\tan\mu) = \frac{1}{\tan\bar{\mu}}\,exp\left(-\frac{\tan\mu}{\tan\bar{\mu}}\right),$$

where pdf(tanμ) is an exponential distribution of the random variable tan μ, and $\bar{\mu}$ is the mean effective friction slope angle). Additional model inputs consist of the digital elevation model and its grid resolution (Δx), initial particle velocity (V_o), number of particles released per pixel (n), mean hop time of a particle (Δt), maximum hillslope length allowed (L_s), a shock term coefficient (κ), and a shock term exponent (α). The latter two inputs control the magnitude of the velocity- (V) dependent shock term (i.e., $\kappa|V|^\alpha$) and whether momentum loss scales with particle velocity ($\alpha = 1$) or particle kinetic energy

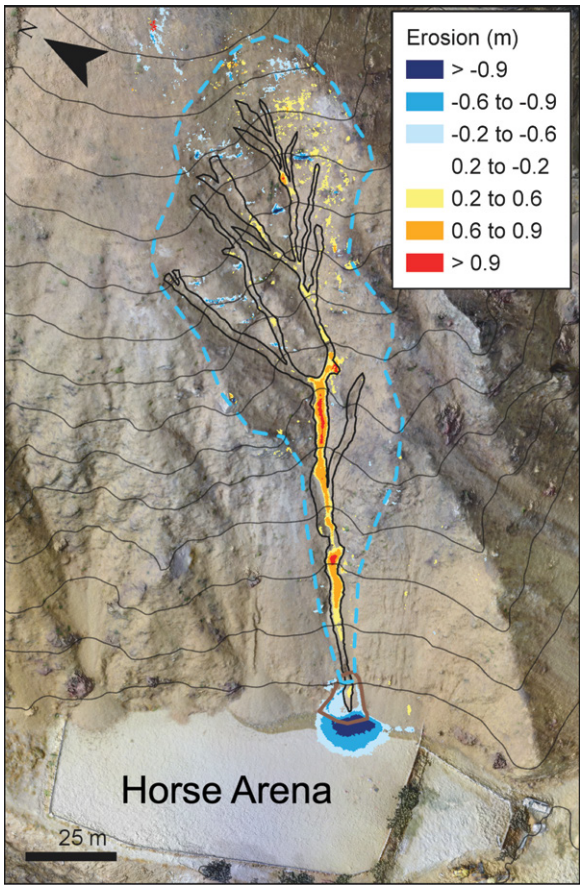

Figure 3. Study site map shows elevation change based on differencing digital elevation models from post-fire and pre-storm (27 October 2016) to after the first major storm (21 December 2016). Any elevation changes within −14 cm to 20 cm are not shown because these are within our uncertainty of no topographic change based on analysis of known points. Warm colors are regions of erosion, and cooler colors are regions of deposition.

($\alpha = 2$) (Gabet and Mendoza, 2012). Following DiBiase et al. (2017), who calibrated the model in a nearby catchment that is similar to our study area, we held $\kappa = 1.6$ and varied α, V_o, and tan $\overline{\mu}$ to determine the conditions where the model reproduced the spatial patterns of ravel accumulation as determined from imagery and field observations (e.g., Fig. 4) and the total volume and thickness of post-fire ravel within the channel and ravel cone. We tested $\alpha = 1$ or 2, V_o of 1.6, 1.7, and 1.8 m/s, and tan $\overline{\mu}$ of 0.36, 0.41, and 0.56. These are within the ranges suggested by DiBiase et al. (2017) based on field and numerical experiments. Our reference DEM (i.e., Survey 1) was used for the ravel simulations, where the post-fire ravel cone on the terrace was removed numerically to determine which model parameters allowed for sediment to transport over long enough distances to build the observed cone deposit. To remove the ravel cone from the DEM, topographic data within the region mapped as ravel cone was eliminated, and the topography was projected laterally from the east and west to create a pre-ravel cone land surface. There was no sediment at the base of the channel prior to the fire due to regular maintenance of the flat horse arena.

To run the ravel model, we followed previous work and assumed that all ravel within the catchment was stored behind vegetation dams (Lamb et al., 2011, 2013), which is plausible as much

Figure 4. Image of field site post-fire and pre-storm (6 October 2016) highlights the steep topography, build-up of ravel cones along the horse arena (terrace), and the infilling of the channel with ravel and minor rilling (inset). The dashed rectangle shows the approximate location of the inset image.

of the hillslope is above the angle of repose (i.e., ~40° to 50°, Fig. 1B), and the catchment was vegetated prior to the fire (Fig. 2). The average sediment thickness on the hillslopes that was released by the fire as dry ravel can be written as $H = cV_s$, where c is the plant stem density per unit area and V_s is the volumetric storage capacity per plant (e.g., Lamb et al., 2011). A value of 0.5 plants/m^2 was used based on nearby vegetation surveys (Keeley, 1992) and was confirmed using image classification techniques (i.e., Normalized Difference Vegetation Index [NDVI]) on a National Agriculture Imagery Program (NAIP) image taken pre-fire (Fig. 2). For simplicity, a vegetation dam width of 1 m was used, following DiBiase and Lamb (2013), which was based on their field observations in the nearby Little Santa Anita Canyon catchment. These estimates of plant storage resulted in an effective thickness of 30 mm of transiently stable sediment averaged over the catchment area. Using the measured dry bulk density of 1.4 g/cm^3 for ravel deposits, and assuming the intact rock density is 2.6 g/cm^3, then the sediment thickness is equivalent to ~1.6 cm of eroded bedrock. With average rates of soil production in the region of ~0.5 mm/yr (DiBiase et al., 2010; Heimsath et al., 2012), this represents ~30 years of soil production, which makes sense as the last fire at the site occurred in 1980.

To estimate peak boundary shear stresses (τ_p) exerted on the hillslope and channel from runoff generated during the 16 December 2016 storm event, we used a simple rainfall runoff approach, assuming steady-state precipitation over the entire catchment. McGuire et al. (2017, 2018) developed a numerical model for predicting runoff and debris flow initiation in steep, post-fire landscapes, which was applied to a nearby catchment (Tang et al., 2019b), but their infiltration model relies heavily on in situ measurements of saturated hydraulic conductivity and the wetting front capillary pressure head, which we did not collect for our site. As such, we chose a simpler approach that requires fewer input parameters, similar to Rengers et al. (2016b). Three different peak 15 min rainfall intensities (P) were modeled, 7 mm/hr, 13 mm/hr, and 18 mm/hr, which corresponded to observed erosion events. Using our reference DEM, surface discharge was calculated in each pixel (q_i) as

$$q_i = cPA_i, \tag{2}$$

where c is a runoff coefficient that accounts for infiltration and evaporation and is a function of soil type, soil water content, drainage basin slope, burn severity, and drainage area among other factors (Dingman, 2015), and A_i (m^2) is the drainage area contributing to the pixel, as determined using the D-infinity method in LSDTopoTools (Tarboton, 1997). As our catchment is steep, has a small drainage area, is relatively smooth due to the lack of vegetation, and is mostly bedrock with a thin and patchy soil cover, we assume that $c = 1$, giving maximum peak shear stress estimates (which would be conservative, for hazard prediction purposes).

From conservation of mass at steady state

$$q_i = h_i b U_i, \tag{3}$$

where h_i is the surface flow depth in each pixel i, b is the width of the pixel (1 m), and U_i is the average flow velocity. U_i was calculated using Manning's equation,

$$U_i = \frac{h_i^{2/3} S_i^{1/2}}{n} \tag{4}$$

where S_i is the tangent of the bed slope angle θ for each pixel, and n is the Manning's roughness coefficient. We used $n = 0.08$ s/m$^{1/3}$ for the entire watershed based on surface flow velocity and depth data from Palucis et al. (2018), who performed steep flume experiments (bed slopes up to 17°) using similar gravel sizes (D_{50} ~5 mm, where D_{50} is the median grain size) and bed morphologies to those found at the field site. Our Manning's n value was also within the range of values used by Tang et al. (2019a) (i.e., 0.03–0.096 s/m$^{1/3}$). Rearranging Equation 3 to solve for h_i and substituting into the predicted maximum shear stress assuming steady and uniform flow conditions (i.e., $\tau_{p,i} = \rho g h_i S_i$ where g is gravitational acceleration and ρ is water density) gives

$$\tau_{p,i} = \rho g q_i^{3/5} n^{3/5} S_i^{7/10}. \tag{5}$$

To test for debris flow initiation by surface runoff, the model of Takahashi (1978) was used, recast in terms of a Shields stress by Prancevic et al. (2014) as

$$\tau^*_{(df,i)} = (1-\eta)(tan\phi_f - S_i) - \frac{\rho}{\rho_s - \rho} S_i, \tag{6}$$

where η is porosity and ϕ_f is the failure plane friction angle, which were set to 0.4° and 47°, respectively, based on our laboratory and tilt table measurements. The non-dimensional shear stress, or the Shields stress, is

$$\tau^*_i = \frac{\tau_{p,i}}{(\rho_s - \rho) g D_{50}}, \tag{7}$$

where ρ_s is the sediment density (2600 kg/m^3). Thus, when the ratio of the Shields stress to the critical value for mass failure for an individual pixel (i.e., $\tau^*_i / \tau^*_{df,i}$) is greater than 1, mass failure of the channel bed is predicted to occur. Equation (6) is a useful quantitative metric for mass failure of the channel bed, and such failures in loose gravel similar to post-fire ravel have been shown experimentally to evolve into landslides, debris flows, or concentrated sheet flows (Prancevic et al., 2014, 2018; Palucis et al., 2018).

FIELD OBSERVATIONS

Post-Fire, Pre-Storm Dry Ravel

The first survey of the study site was conducted following the Fish Fire, which occurred in June/July 2016 before the first large winter storm in December 2016. At this time, only low relief, dry granular flow chutes on hillslopes were observed with no evidence of slumping or landsliding. There were thin ravel deposits on the hillslope (<5 cm), as well as thicker, loosely consolidated ravel deposits within the channel network with charred organics (e.g., 41 ± 15 cm at the apex of the ravel cone on the terrace and 31 ± 10 cm at the knickpoint). A ~4 m^3 ravel cone (~77 m^2) was built at the exit of the channel onto the floor of the horse arena (outlined in brown, Fig. 1A). The ravel cone was at the angle of repose (~37°) and was composed of loose silt, sand, some gravel, and burned plant material (black line, Fig. 5). Approximately a dozen decimeter-scale blocks of bedrock were scattered on the outer edges of the cone (black arrows, Fig. 5B), likely derived from rock fall from outcrops above. Remaining plants on the hillslopes included burned and damaged chaparral and yucca plants, and the ground had a slight hummocky appearance at the meter scale due to both bedrock outcropping and remaining soil mounds from root balls of incinerated plants.

Sediment Transport during the December 2016 Storm

The December 2016 storm was a convective storm that started around 18:10 on 15 December and lasted ~28 h, ending at 12:25 on 16 December (Fig. 6). In total, 60 mm of rain fell at the site with a peak 15 min rainfall intensity of 28 mm/hr. This storm was typical of the region, with a recurrence interval of 1 yr, based on the San Gabriel Canyon weather station ~2 km east of the site (Station 04–7776, Precipitation Frequency Data Server, National Oceanic and Atmospheric Administration). At the start of the storm at ~18:10 on 15 December, when rainfall intensities were ~1 mm/hr, sediment movement was observed within the channel via rain splash impacts at our upper camera site, but there was no observable deposition at the lower camera site. As rainfall rates increased to ~3 mm/hr at 19:41, overland flow was observed at the bedrock knickpoint with no visible rilling or scour of the channel infill. During this same time, rain splash impacts were observed on the ravel cone.

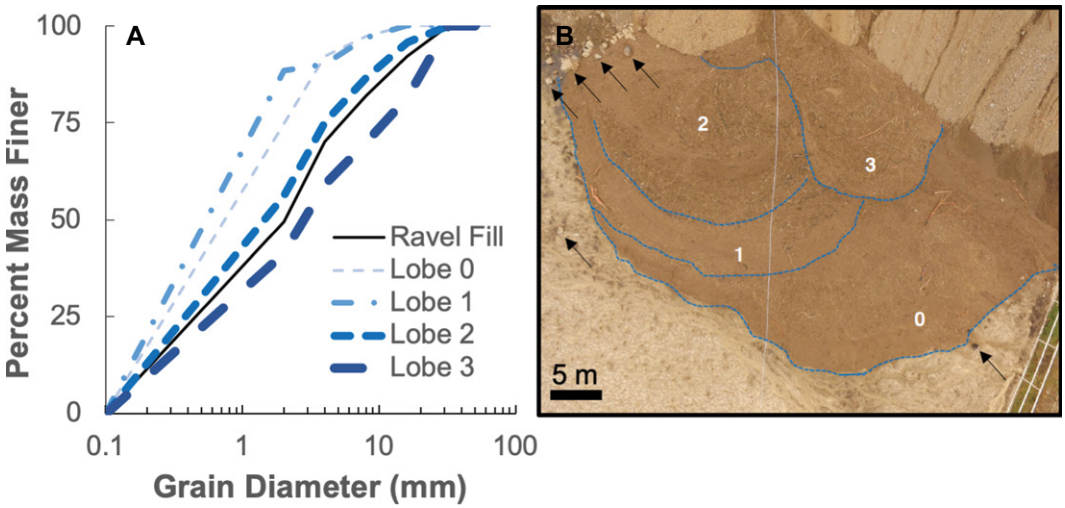

Figure 5. (A) Grain size distribution of post-fire and pre-storm ravel deposits (black line, collected at the red square in Figure 1A on 27 October 2016) is shown. Grain size distributions are also shown for four post-storm sediment lobes on the debris flow fan, the locations of which are shown in the downward-looking image in panel B. (B) Lobe 0 was deposited early in the storm, and Lobe 3 represents the final stage of deposition. Arrows indicate the locations of decimeter-scale boulders.

Shallow flow over the ravel cone carrying plant material can also be seen during this time but with no observable rills on the cone. Rainfall intensities decreased to ~1 mm/hr at 19:56.

Rainfall intensities increased several times between 00:05 and 03:15 with peak 15 min intensities of ~8 mm/hr. Between ~00:05 and ~00:55 (Event E1, Fig. 6), increased overland flow was observed at the upper camera site, which resulted in the formation of small rills within the channel fill (Figs. 7A–7B) as well as on the ravel cone at the channel mouth (Figs. 7C–7E). This event corresponded to the formation of a small lobe deposit on the ravel cone (Fig. 7E). Following this surge in rainfall intensity to 8 mm/hr, the intensity of the storm diminished for a short period before briefly increasing to 5.6 mm/hr at 02:16. This small peak in intensity had no corresponding erosion visible in the upper camera nor visible overland flow over the knickpoint.

Rainfall intensity increased again at 04:28 before peaking at a 15 min rainfall intensity of 28 mm/hr at 04:57. During this time, the majority of the sediment within the channel near the bedrock knickpoint was eroded, and significant deposition occurred at the channel mouth to build a fan (Event E2, Fig. 6). The first observable movement of sediment within the channel appeared to have occurred as a result of overland flow cascading off of the bedrock knickpoint, which removed sediment through both sheetflow and jet scouring (Fig. 8A). A plunge pool also formed just downstream of the bedrock knickpoint (Fig. 8B). At the peak in rainfall intensity, mass failure of the channel bed was observed downstream of the knickpoint (Fig. 8C). After failure, the plunge pool below the knickpoint also deepened. Since the storm occurred at night, we could not determine whether the plunge pool scour was due to dilute water flow or a debris flow. On the debris flow fan, continued deposition was observed (Figs. 8D–8E), which occurred through pulses of channel incision near the fan apex and discrete pulses of lobe construction on the distal part of the fan. Storm intensity then decreased around 05:10, reaching lows of 0.8 mm/hr at 05:40.

The storm provided one last pulse of rainfall between 08:37 and 09:14 on 16 December that caused observable erosion and deposition (Event E3, Fig. 6) as rainfall intensity increased from 2.4 mm/hr to 13.6 mm/hr. This pulse resulted in dilute overland flow cascading over the bedrock knickpoint with no observable erosion (Fig. 9A). However, pulses of dilute overland flow and debris flows were observed just upstream of the fan deposit as well as continued deposition on the fan (Figs. 9B–9C). Table 1 summarizes the three observed sediment transport events over the course of one storm, which resulted in evacuation of sediment in the channel and deposition of a fan.

Five days following the 15 December storm, we visited the site and observed minor rilling on the upper hillslopes with no evidence of shallow- or deep-seated landsliding. Much of the ravel infill within the channel had been evacuated, and in some places scour was up to ~2 m deep (Figs. 10–11). The channel contained some pre-fire coarser grained material, which was observed post-storm after much of the ravel had been evacuated, but we lacked a sufficient resolution pre-fire DEM to determine its volume. Erosion was concentrated in the portion of the channel downslope of the bedrock knickpoint toward the center of the channel (red region, Fig. 3); upslope of the knickpoint, the channel remained relatively unchanged.

Four distinct lobes within the debris flow fan (~336 m^2) were mapped in the field (Fig. 5B), where lobe 0 formed early in the storm. Trenching and sampling the fan showed a general upward coarsening trend (Fig. 5A), where the fine-grained ravel was deposited first and the storm-mobilized deposits became progressively coarser, likely due to the entrainment of the coarser, pre-fire sediment from the channel bed. Lobe 0 had a mean surface slope of ~1.5°, lobes 1 and 2 were ~5°, and lobe 3 was ~10°, all of which were much less steep than the ravel cone (~37°) at this location prior to the storm. The lobe deposits were predominately poorly sorted

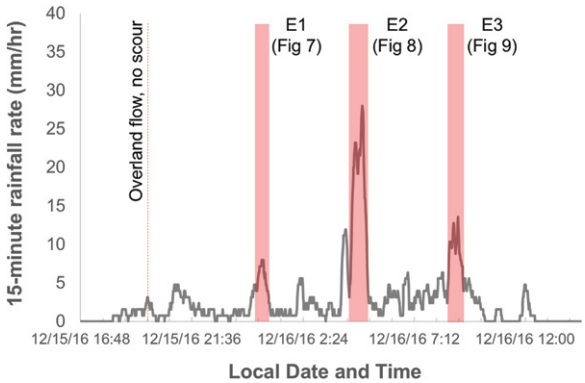

Figure 6. Timeline shows 15 min average rainfall intensities collected by the U.S. Geological Survey gage (Lower Station, Tang et al., [2019b]) over the course of the 15 to 16 December 2016 storm event. Periods of significant erosion and deposition (E1, E2, and E3) that we observed with time-lapse cameras are highlighted in red.

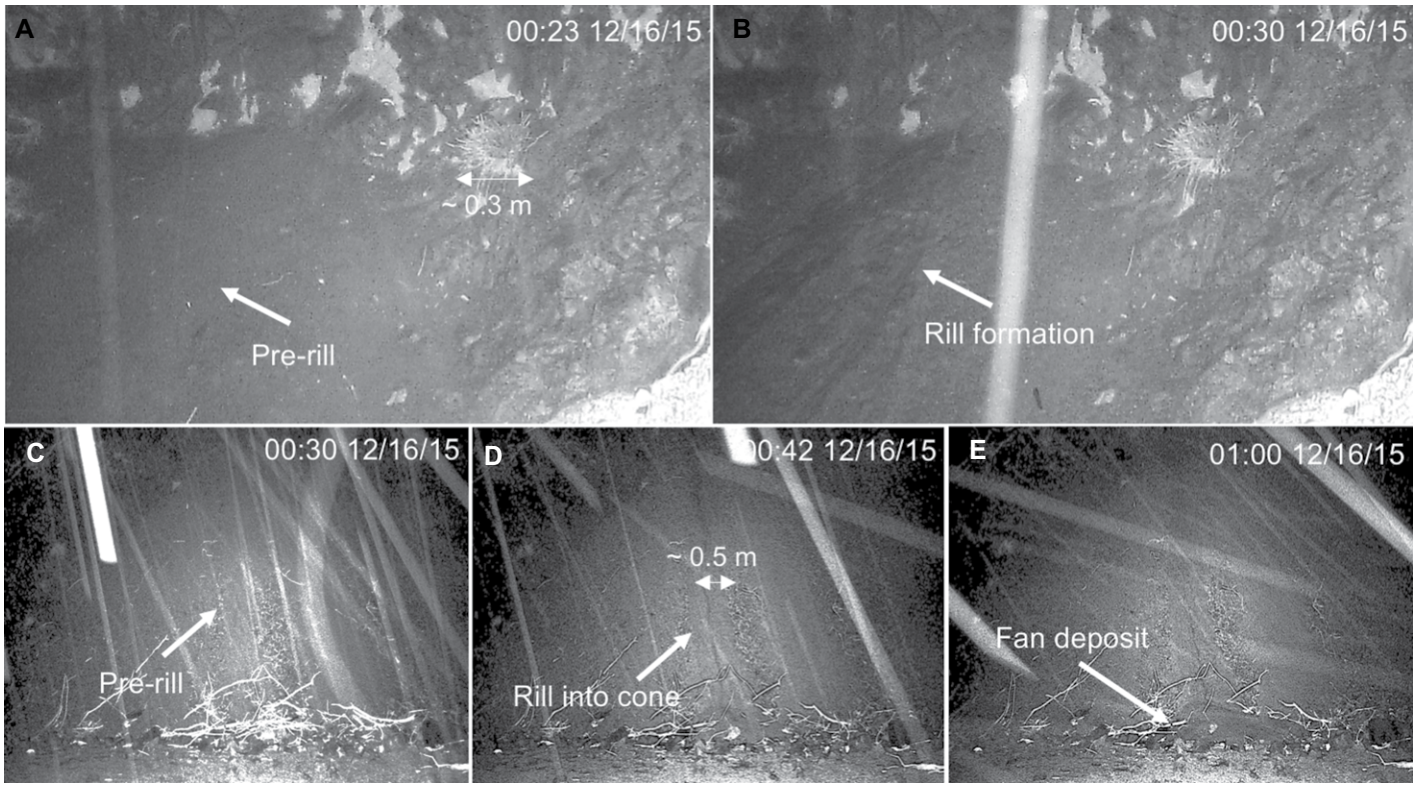

Figure 7. Images taken by time-lapse cameras during event E1 (Fig. 6) are shown. (A) and (B) are from camera C3, which is at the base of the knickpoint in the upper channel (Fig. 1A), at 00:23 and 00:30 on 16 December, respectively, and show the development of rills on the channel fill just downslope of a bedrock knickpoint. Images (C), (D), and (E) (taken at 00:30, 00:42, and 01:00 on 16 December, respectively, by camera C2 on the terrace) show the progressive incision of the pre-storm ravel cone and the initial deposition on the fan (highlighted in tan). The bright lines in front of the fan are sticks and organic material that were transported downslope in the storm event.

coarser clasts within a fine-grained matrix, supporting the photographic evidence that the main flows that built the fan were debris flows. We did observe some clast-supported deposits of relatively uniform sized grains (approximately pebble sized) interbedded between debris flow deposits, which were likely deposited fluvially or by sheetflows.

Based on the topographic surveys (Fig. 3), $\sim 81.5 \pm 23$ m^3 of sediment was removed from the channel during the storm event, and $\sim 85.5 \pm 2.5$ m^3 was deposited in the ~ 336 m^2 debris flow fan, which almost completely overtopped the 77 m^2 ravel cone, where the remaining sediment was likely from hillslope rills and rockfall. Thus, our result shows that ~95% of the material deposited in the fan was sourced directly from the channel.

Throughout the rainy season we continued to visit the field site and collect UAV imagery to document qualitatively how the catchment evolved. Following the 15 December storm, several storms occurred, including a larger event on 20 January 2017 (Fig. 12). This storm had a peak intensity of 33.6 mm/hr and resulted in a large debris flow within Van Tassel Canyon (~2.5-m-deep flow and capable of carrying meter-scale boulders) that washed out the entire horse arena and entrained the fan we had been monitoring (Tang et al., 2019a, 2019b). However, as most of the finer-grained channel infill already had been eroded from our study site in the previous storms, little additional erosion of our catchment was observed either in the channel, where only exposed bedrock and coarser, pre-fire basal sediments remained, or through additional or deepening rilling or landsliding on the hillslope.

ANALYSIS

Sediment Transport by Dry, Granular Flow

Observations of post-fire, pre-storm ravel accumulation were used to both calibrate the model of DiBiase et al. (2017) for post-fire landscapes and to provide estimates of ravel thicknesses across the entire catchment. Independent of the chosen effective mean friction angle, the model predicts that ravel does not accumulate on the portion of the catchment mapped as hillslope (Fig. 13), consistent with our field observations and measurements. The model predicts that ravel does accumulate in convergent portions of the catchment, which corresponds to the channel network. The predicted thickness of the ravel in a given portion of the channel and the size of the ravel cone on the terrace depend on the specified mean granular friction angles, $\tan\bar{\mu}$. For example, for $\tan\bar{\mu} = 0.36$ (corresponding to the low friction end-member), ravel is not predicted to accumulate at the channel heads, and instead much of the deposition is concentrated just upstream and downstream of the small bedrock knickpoint or on the terrace (Fig. 13A). For this value, the model overpredicts the volume of the cone (i.e., 4.4 m^3 versus measured 3.9 m^3) and overpredicts the total ravel infill within the mapped channel perimeter (104 m^3 versus the observed 81.5 m^3). For greater $\tan\bar{\mu}$, deposit thicknesses are lower and more uniform across the entire channel domain, and deposits extend higher up into the channel network, which is more similar to our observations (Figs. 13B–13C). The model scenario that best matches our measured ravel cone volume is with $\tan\bar{\mu} = 0.41$; for greater friction angles, the model under-predicts the cone volume (e.g., 3.2 m^3 for $\tan\bar{\mu} = 0.56$). A friction

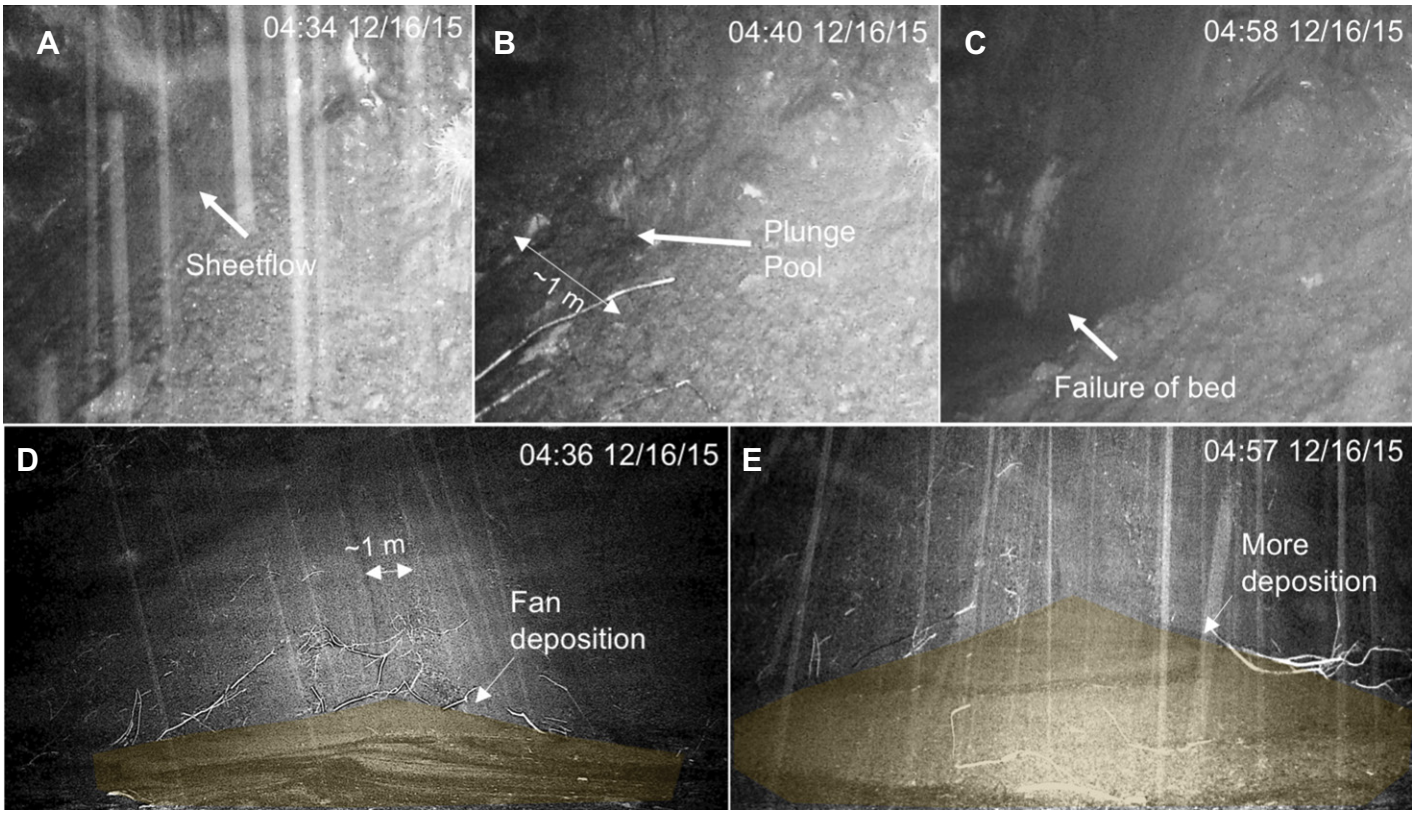

Figure 8. Erosion and deposition occurring during event E2 (Fig. 6), where (A), (B), and (C) are images taken by camera C3, at the base of the knickpoint in the upper channel (Fig. 1A), at 04:34, 4:40, and 4:58 on 16 December, respectively, showing the onset of sheetflow, the development of a plunge pool, and eventual failure of the bed. Images (D) and (E) (taken at 04:36 and 04:57 on 16 December, respectively, by camera C2 on the terrace) show the continued development of a debris flow fan (highlighted in tan).

value of tan $\bar{\mu} = 0.41$ produces a total ravel fill in the channel of 78 m^3, which brackets our observations. However, the model underestimates our two local measurements of ravel infill depths in the channel of 25.4 cm and 40.6 cm (white dots on Fig. 13); the model predicts depths of 12 cm and 13.2 cm for the upslope and downslope sites for tan $\bar{\mu} = 0.56$, 15.6 cm and 18.6 cm for tan $\bar{\mu} = 0.41$, and 18 cm and 18.6 cm for tan $\bar{\mu} = 0.36$. This underestimate could be due to channel deposits that existed before the fire or because the model assumed that the unstable soil on the hillslope was uniform, whereas in reality it likely varied across the catchment, which led to locally thicker or thinner ravel deposits within the channel.

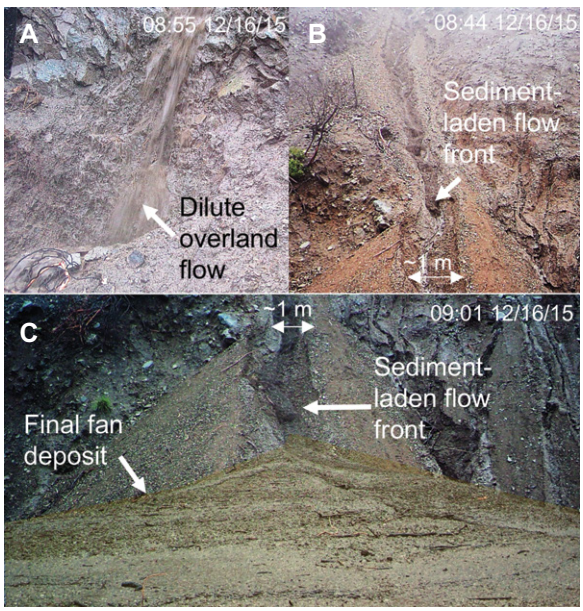

Figure 9. Erosion and deposition occurring during E3 (Fig. 6), where (A) was taken by camera C3 at the base of the knickpoint in the upper channel (Fig. 1A) at 08:55 on 16 December, showing dilute overland flow occurring over the bedrock knickpoint. Image (B) was taken at 08:44 on 16 December by camera C1 and shows a debris-flow front at the apex of the fan that likely initiated downslope of camera C3. Image (C) was taken at 09:01 on 16 December by camera C2, on the terrace, and shows the final stages of development of the fan.

In-Channel Failure by Runoff

Dry ravel at our field site was dominated by very coarse sand/fine gravel ($D_{50} = 2.1$ mm, $D_{16} = 0.25$ mm, and $D_{84} = 10$ mm) (Fig. 5), which is finer-grained than the cobbles and boulders that typically line the first order channels in our study area (DiBiase, 2011). Although we did not survey the channel bed prior to it being filled with ravel, observations during the storm event revealed a basal layer of gravel and cobbles that was coarser than the post-fire ravel and likely accumulated before the fire. For the same runoff event, finer grain sizes have larger Shields numbers, which makes failure of channel beds with fine grains more likely (Prancevic et al., 2014). Unlike debris flows triggered by landslides,

TABLE 1. SUMMARY OF THE THREE OBSERVED SEDIMENT TRANSPORT EVENTS DURING DECEMBER 2016 STORM

Event no.	Start time and date of event	Event duration (min)	Average rainfall rate (mm/hr)	Observations
E1	00:27 15 December 2016	~24	6.8	Minor rilling of channel fill and corresponding deposition of a debris lobe.
E2	04:20 16 December 2016	~42	18.1	Sediment failure of the channel bed, transport by sheetflow and debris flow, deposition of a debris flow fan.
E3	08:37 16 December 2016	~30	13.3	Continued deposition on the fan from clear and sediment-laden flows; inferred sediment erosion occurred mid-channel.

in-channel debris flow initiation in the presence of overland flow is a strong function of sediment size (Prancevic et al., 2014; Palucis et al., 2018).

Figure 14 shows results from our steady state rainfall runoff model, where pixels highlighted in red signify where the ratio of the Shields stress to the critical Shields stress for mass failure ($\tau_i^*/\tau_{df,i}^*$) is greater than unity. For the three modeled peak rainfall intensities, there appears to be positive correlation between observed erosion locations during the December 2016 storm (warm colors, Fig. 3) and predicted in-channel failure (red pixels, Fig. 14). For peak rainfall intensities of 7 mm/hr, failure was not predicted to occur within the channel or on the hillslope, consistent with our observations during event E1 (Table 1). For peak rainfall intensities of 13 mm/hr (Fig. 14A), <5% of the catchment and ~20% of the channel was predicted to fail due to runoff. This percentage increased to ~40% of the mapped channel network for peak rainfall intensities of 18 mm/hr (Fig. 14B), which is consistent with our observations of debris flow initiation during event E2 (Table 1). Areas prone to failure are those that concentrate flow (i.e., high drainage area; Fig. 14), which also corresponds to regions that accumulate dry ravel (red shaded regions, Fig. 13). Although the predicted zones of initial failure are small compared to the entire channel length, experiments have shown the initial zones of failure can rapidly grow to evacuate the entire sediment bed (Prancevic et al., 2014, 2018).

DISCUSSION

Debris Flow Initiation: Hillslope or Channel?

We set out to test whether hillslope versus in-channel initiation mechanisms lead to debris flow occurrence in steep, post-fire terrain where few direct measurements exist. One hypothesis is that debris flows initiate on hillslopes due to changes in hillslope soil properties that increase runoff, such as increased hydrophobicity (e.g., MacDonald and Huffman, 2004), clogging of soil pores with ash (e.g., Woods and Balfour, 2010), or extreme drying of the upper soil (e.g., Burch et al., 1989), all of which are thought to vary with burn severity (e.g., Certini, 2005). Then, during high intensity storms, concentrated runoff develops on hillslopes due to decreased infiltration, leading to shallow mass failures of the soil surface, which can progressively entrain material and transform into debris flows (Gabet and Bookter, 2008). Meyer et al. (2001) observed a shift from debris flow initiation by surface runoff processes to debris flow initiation by shallow landsliding over the course of several years in the Idaho batholith region, which they suggest is not due to regrowth of herbaceous vegetation but to loss of deep-root strength. This shift has also been documented across portions of the San Gabriel Mountains, likely due to increasing soil infiltration capacity (Rengers et al., 2020).

While the aforementioned hillslope processes for post-fire debris flow initiation may dominate in portions of the landscape with continuous, thick, stable soil mantles, they do not appear to be applicable in the small, steep, first-order bedrock catchment in our study area, where greater than 50% of the hillslope has exposed bedrock. We did not observe major rilling on the hillslopes draining to our channel network or evidence for mass wasting on the hillslope in the form of local soil scars, slip faces, or headscarps from shallow landsliding. However, there was significant dry ravel present after the fire, which often manifested as ravel cones or fans at the base of a slope. As such, the "burn-ravel

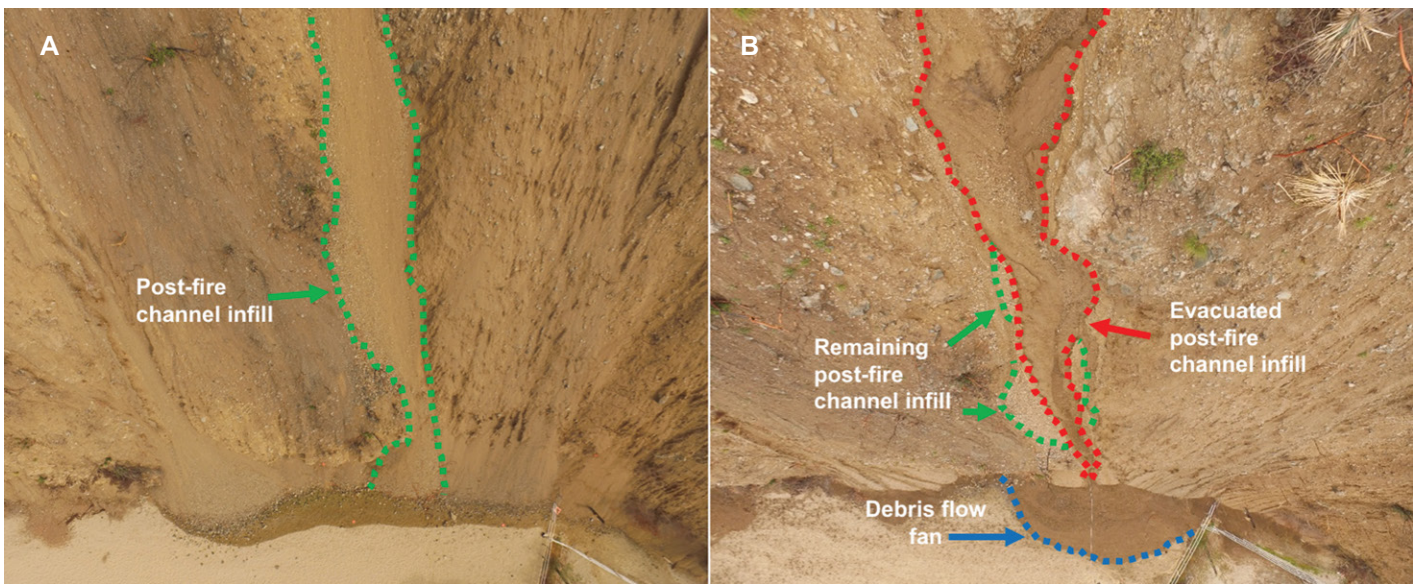

Figure 10. (A) Downward-looking unmanned aerial vehicle (UAV) image taken on 27 October 2016 showing channel infill post-fire and pre-storm. (B) Similar downward-looking UAV image taken on 21 December 2016 showing where channel infill was excavated and deposition of the debris flow fan overlying the horse arena.

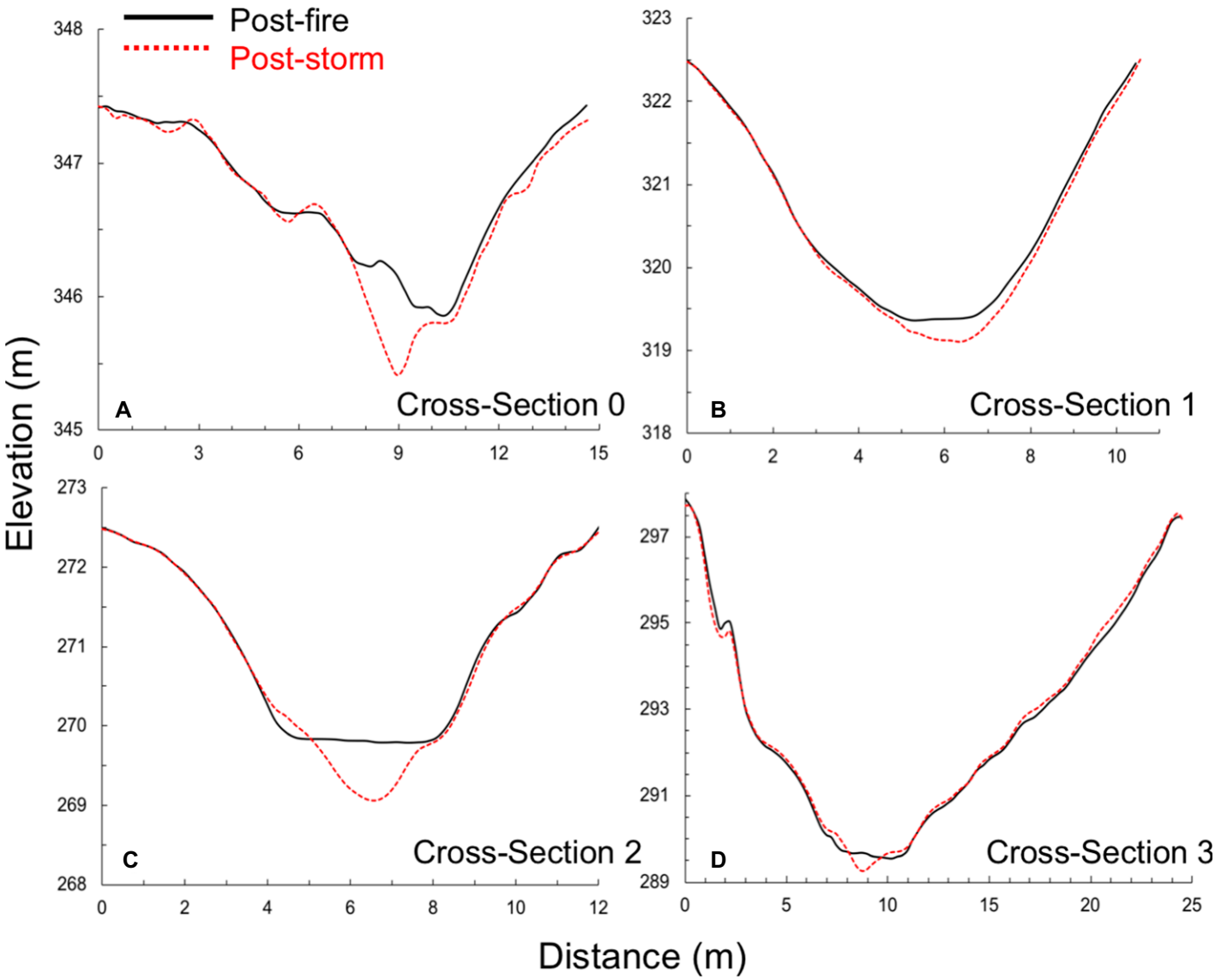

Figure 11. (A–D) Cross-sections extracted from pre- and post-storm digital elevation models at four locations along the channel network are shown (see locations in Fig. 1A).

release–in-channel failure" mechanism that has been proposed previously appears more appropriate. In these steep, rocky catchments, vegetation acts as a sediment trap, allowing patchy soil cover to develop above the angle of dry soil stability (e.g., DiBiase and Lamb, 2013), and once that vegetation is destroyed by fire, the sediment is rapidly transported by gravity alone to convergent zones and channels though dry ravel (Florsheim et al., 1991; Gabet, 2003; Lamb et al., 2011; DiBiase et al., 2017). This sudden influx of relatively fine-grained sediment (median grain sizes are often <2 mm) to steep channels, combined with concentrated runoff over bare bedrock, leads to debris flows, hyper-concentrated flows, and possibly sheetflows that initiate in-channel (Eaton, 1935; Takahashi, 1978; Wells, 1987; Kean et al., 2011; Prancevic et al., 2014; Palucis et al., 2018).

Our field observations, mass balance closure, and modeling support this second hypothesis. We observed that ~1 month after the fire, but before any rainfall, the channel at our site was buried in ravel and a relatively large (~4 m^3) ravel cone had developed at its base. Neighboring channels were similarly filled with ravel and had ravel cones extending from their outlets. Based on estimates of pre-fire vegetation density and a ravel model, we showed that much of the sediment that had been generated over the past 30 years and stored behind vegetation dams is predicted to have accumulated in the channel network once the vegetation was burned, as was observed. Moreover, the convergent channel network where dry ravel is predicted to have accumulated (Figs. 4 and 13) is also the area where significant erosion was observed during storms. As such, the steep channel network studied here is only a temporary sink for post-fire hillslope sediment. As observed during the December 2016 storm event, in-channel runoff, likely generated on the bedrock outcrops in the upper portion of the catchment, was able to entrain and evacuate sediment as debris flows through channel bed failure (Fig. 8). We show from mass balance that 95% of the sediment deposited in the fan was derived from the ravel-filled channel with the remainder coming from the hillslope.

It is useful to compare our findings to other studies on post-fire sediment transport in steep catchments. DeLong et al. (2018) used

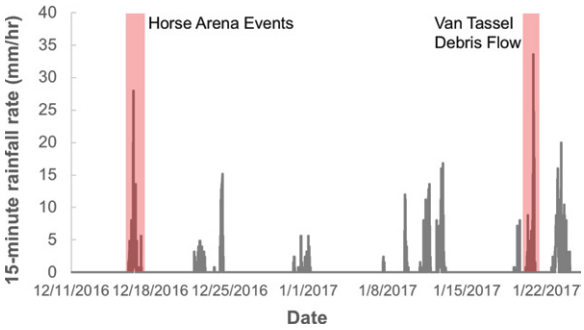

Figure 12. Timeline shows 15 min average rainfall intensities collected by the U.S. Geological Survey gage (Lower Station, Tang et al. [2019]) over the course of winter 2016–2017. The rainfall events leading to erosion and deposition at the Encanto field site, as well as the large debris flow event in Van Tassel Canyon on 20 January that overtopped the horse arena, are highlighted.

repeat terrestrial laser scanning in a 75,000 m^2 catchment in the Chiricahua Mountains in southeastern Arizona and found that the first post-fire precipitation event led to sediment yields where ~69% was from hillslope erosion and ~31% was generated from a gully channel established in colluvial hollows. This rain event lasted ~2 h, with peak 10 min intensities of 82 mm/hr and 49 mm/hr and a total rainfall of 70 mm. The storm resulted in the formation of extensive rills and gullies, suggesting that overland flow occurred within the catchment and that sediment-laden flow, possibly debris flow, was generated. Basin slopes were reported to be in excess of 30°, and the overall drainage basin slope was 40°, but the authors did not observe significant dry ravel processes as there were no debris cones and/or aprons and the hillslope soils post-fire were gravitationally stable (DeLong et al., 2018). Rengers et al. (2016a) conducted a similar study, measuring erosion of a burned area over the course of several storms in the Colorado Front Range. The study site had lower slopes between 17° and 30°. For 10 min peak rainfall intensities similar to those that occurred at the DeLong et al. (2018) site (i.e., ~72 mm/hr), Rengers et al. (2016b) observed extensive rilling and surface erosion from overland flow but no dry ravel or debris flow generation, and they found that most of the sediment yield (~87%) was generated from hillslopes and not from the channel. Staley et al. (2014) worked in a similarly sized basin (0.01 km^2 versus 0.006 km^2) within the San Gabriel Mountains, where they divided the catchment into process domains (i.e., hillslope-divergent, hillslope-convergent, transitional, and channelized incision) and found that most sediment yield was contributed by the hillslope-divergent (57%) and hillslope-convergent (36%) domains, and that raindrop-impact induced erosion, dry ravel, surface wash, and rilling all contributed to debris flow initiation. In contrast to our site, their site was burned at moderate to high severity, has a lower median basin slope (~39° versus ours at 44°), and a lower channel slope (~22° versus 30°). While all of these catchments studied are relatively small and steep and experienced similar peak rainfall intensities (~30–70 mm/hr), our catchment is distinct in that most of the terrain (~83%) is steeper than the angle of dry sediment stability (i.e., >37°). Because dry ravel is inherently a threshold process (Gabet and Mendoza, 2012; DiBiase et al., 2017; DiBiase and Lamb, 2020),

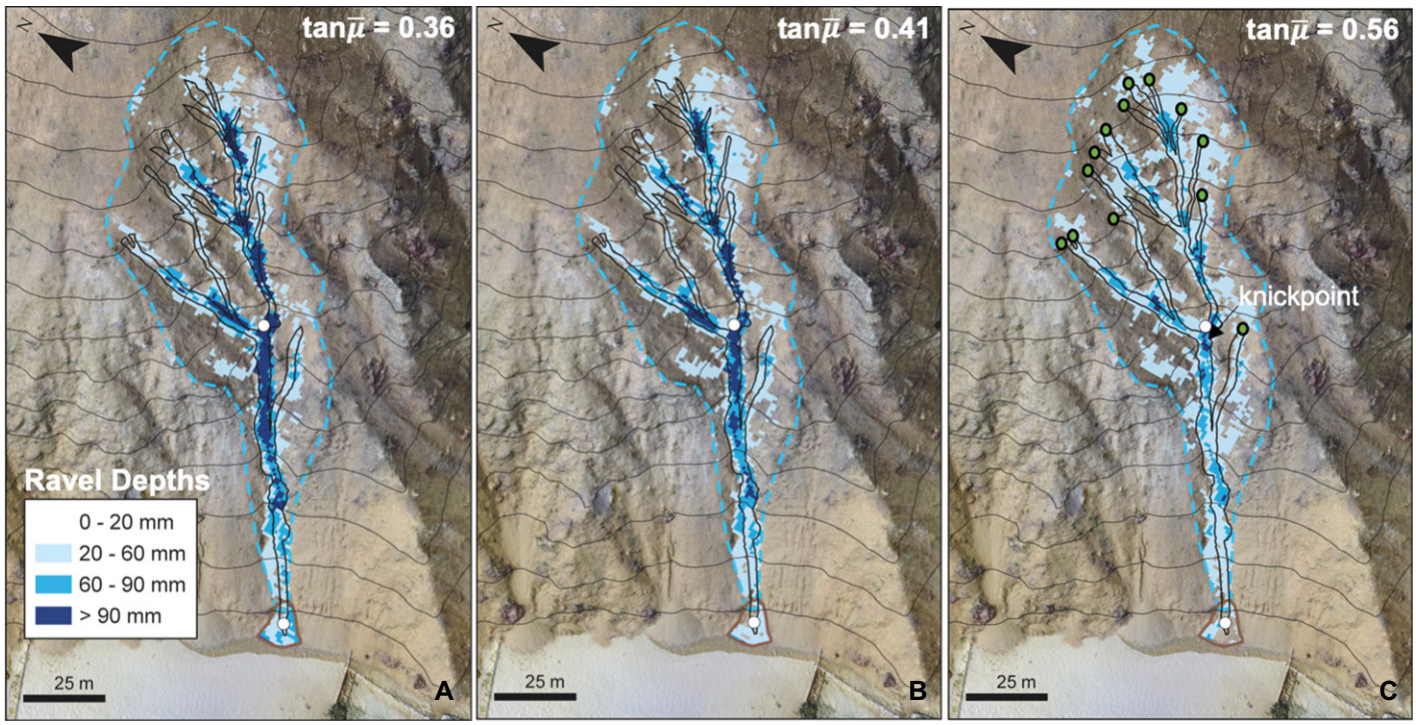

Figure 13. Ravel model output based on the model of DiBiase et al. (2017) is shown, where all parameters are held constant between runs (see text) except for the mean friction slope, where for (A) tan$\bar{\mu}$ = 0.36, (B) tan$\bar{\mu}$ = 0.41, and (C) tan$\bar{\mu}$ = 0.56. The three process domains are mapped: the channel network (outlined in black), the hillslope (outlined with blue dashes and not including the channel network), and the depositional domain (ravel cone outlined in brown). White dots show the locations of ravel depth measurements. We also show the location of the channel heads (green dots) and the knickpoint (arrow) in (C).

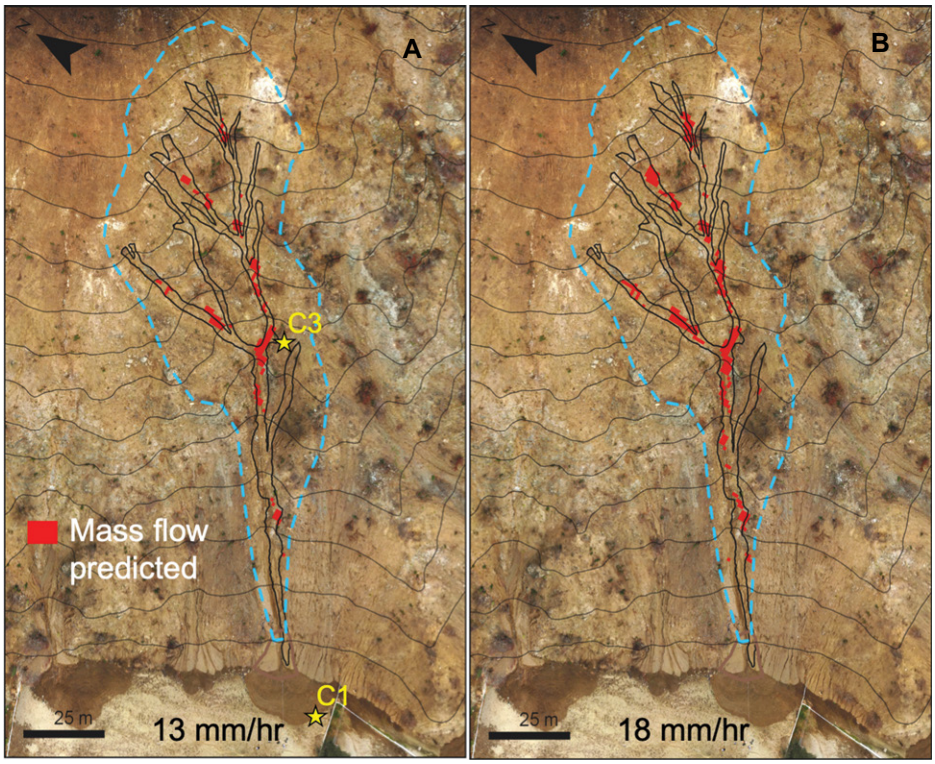

Figure 14. Rainfall-runoff model output with average rainfall intensities of (A) 13 mm/hr and (B) 18 mm/hr is shown. Regions colored in red are where modeled Shields numbers exceed the critical Shields number for in-channel mass flow initiation (which we infer leads to debris flow initiation). The three process domains are mapped: the channel network (outlined in black), the hillslope (outlined with blue dashes and not including the channel network), and the depositional domain (ravel cone outlined in brown). The time-lapse cameras are marked with yellow stars.

the steeper slope of our catchment can explain the much different post-fire sediment transport mechanisms. In particular, instead of hillslope runoff erosion, we observed hillslope sediment transport occurring principally by dry ravel, debris flow initiation occurring by channel bed failure, and 95% of the rainfall-induced sediment yield driven by evacuation of channel fill.

In agreement with our findings, Tang et al. (2019b) studied a 0.12 km^2 drainage basin just upslope of our site (also within Van Tassel Canyon) following the same fire and also found that ravel-filled channels were commonly dominant debris flow sources. They used the model of McGuire et al. (2016, 2017), which, compared to our approach, included a more complex water routing algorithm, hillslope runoff and soil erosion modeling, and a Mohr-Coloumb approach for channel bed failure similar to that of Prancevic et al. (2014). While Tang et al. (2019b) did not model dry ravel dynamics, they did observe ravel fills in low order channels and imposed these fills as an initial condition in their model (initial thickness of 0.47 m, which is similar in scale to our observations). Some of their modeled events produced significant hillslope erosion, but they concluded that mass failure of ravel-filled channel beds was the most important mechanism for debris flow initiation. Their Storm 1 was actually the same storm event that we monitored; while they found nearly equal contributions of hillslope and channel sediment in their catchment for this event, we found that almost all erosion (~95%) occurred within the channel. This difference could be due to the lower mean hillslope angle of their catchment (i.e., 38° versus ours at 44°)—implying greater hillslope sediment stability in their catchment. Tang et al. (2019b) also assumed their catchment was soil-mantled for hillslope angles less than 45°; however, our results, and previous field and modeling work (e.g., DiBiase et al., 2017; DiBiase and Lamb, 2020), suggest that soils can be gravitationally unstable on hillslopes with angles as small as ~30° following the incineration of vegetation dams. This terrain, with slopes of ~30° to 45°, is the most likely source of dry ravel (DiBiase and Lamb, 2013; Lamb et al., 2013), implying a hillslope sediment supply limitation for runoff-driven erosion that may not have been included in previous models. We also defined hillslope and channel domains differently; they used a contributing area threshold of 1000 m^2, whereas we mapped channel heads visually, resulting in much smaller contributing areas that ranged from 0.1 m^2 to 100 m^2 (Fig. 1C).

In-Channel Debris Flow Initiation Mechanisms

Using the model of Takahashi (1978) and Prancevic et al. (2014) (which is also similar to that used by Tang et al. [2019b] and McGuire et al. [2016, 2017]), combined with a simple rainfall runoff model, we found good correspondence between the zones of predicted failure and the observed regions of erosion in the channel network (Figs. 3 and 14). The model does not predict failure on the hillslope, consistent with our observations, owing to very small drainage areas and, hence, little flow accumulation and runoff (Fig. 3). The model for in-channel failure can also explain why debris flows are so common following wildfire even during modest storm events that typically do not trigger debris flows. Low-order channels are locations of topographic convergence, where both unstable hillslope soil is deposited by dry ravel after fires and where water converges during storms, resulting in high shear stresses from overland flow. Unlike debris flows generated by landslides on hillslopes, channel bed failure in the presence of surface flow is sensitive to sediment size (Equation 6), and the abrupt fining of the river bed due to ravel infill can cause Shields numbers to exceed the threshold for debris flow initiation even for the one-year recurrence interval storm that we monitored.

While the Takahashi (1978) model assumes steady and uniform flow over the sediment bed, the flow was unlikely steady and uniform in our study area, at least not immediately downslope of the bedrock knickpoint, where jet and plunging flow was observed under some of the highest peak rainfall intensities. Debris flow initiation could have occurred through failure of sediment accumulated at the downstream margin of the pool (Kean et al., 2013) or by the impinging jet similar to the "fire hose" effect as conceptualized by Johnson and Rodine (1984). Scheingross and Lamb (2016) also observed a similar phenomenon during flume experiments; when plunge pools aggraded to shallow pool depths (~<5 cm), they observed bed fluidization and significant grain-grain interactions. Observations from the upper camera (Fig. 8), as well as sheetflow-like deposits in the debris flow fan, suggest that granular sheetflows occurred in conjunction with debris flows. The channel slope downstream of the knickpoint is ~20°, a

moderately steep slope that is just shallower than the transitional slope between debris flow initiation and the onset of fluvial transport observed in experiments (Prancevic et al., 2014). These channel gradients are where we may expect granular sheetflow to occur based on flume experiments from Palucis et al. (2018).

Implications for Debris Flow Prediction

Our observations suggest that debris flow hazards in steep, bedrock landscapes can be predicted by combining a vegetation sediment storage model (e.g., Lamb et al., 2011), a ravel routing model (DiBiase et al., 2017), and a channel bed failure model (Prancevic et al., 2014). These models predicted the location of post-fire ravel accumulation as well as where erosion was observed during the December 2016 storm (Figs. 3 and 14). They can also be used to assess the relative amount or volume of sediment that will be brought downstream, likely into higher order channels, as a debris or sediment-laden flow. For example, DiBiase and Lamb (2020) used topography from repeat airborne lidar to track sediment following the 2009 CE Station fire and showed up to 3 m of ravel loading in headwater channels post-fire and before rainfall and up to 5 m of channel erosion from storms in subsequent years. Importantly, most of the catchments where they observed dry ravel accumulation and channel erosion had areas that range from 10^3 m^2 to 10^5 m^2, the same scale as at our study basin, suggesting that observations within our basin are applicable over large regions. The addition of a channel bed failure model would allow one to classify where failure by sediment-laden flow is both likely and where (and how much) sediment is available to fail.

Two important implications of our work relate to the effect of fire frequency on soil production rates and the impact of fire frequency on sediment yield, which is a concern for sediment management. Over longer timescales, and of importance for landscape evolution modeling, fires have been argued to increase soil production rates by thinning soils, leading to smaller hillslopes for the same uplift rate (Roering and Gerber, 2005). However, in bedrock-dominated landscapes it is not clear what sets soil production rates, but the potential feedbacks with soil thickness are likely less important (Heimsath et al., 1997, 2012). Our results suggest that for the bedrock case, a pulse of sediment yield is not tied to a pulse of sediment production but rather to the modulation of sediment storage and release by plants (Lamb et al., 2011, 2013). In regard to sediment yield post-fire, for soil-mantled landscapes that have an inexhaustible supply of relatively stable soil, more frequent fires will result in more sediment yield and hazards. In bedrock landscapes, our results suggest that more frequent fires in a warming climate may not necessarily lead to increased sediment yields due to supply limitations (Lamb et al., 2011). Thus, fire history matters, as does the timescale for replenishing vegetation dams with sediment, the latter of which is set by both plant regrowth and soil production rates.

Much of the available sediment was evacuated from our study site during the first winter storm, which was a typical storm with a one-year recurrence interval. During subsequent larger storm events, which had 1–2-year recurrence intervals, minimal erosion and deposition occurred at our site because the sediment supply was exhausted. However, higher order channels, which were likely loaded with sediment from low order channels following the first storm, produced large debris flows during subsequent storms such as the large debris flow event through Van Tassel Canyon on 20 January (Tang et al., 2019b, 2019a). Thus, the pulse in post-fire sediment may move through the catchment in discrete transport steps: (1) from hills to first-order channels by dry ravel following fire, (2) from first-order channels to higher-order channels during relatively small, early wet-season floods, and (3) from higher-order channels during subsequent larger floods. Repeat lidar after post-fire storm-events to track sediment movement is needed to test this hypothesis (DiBiase and Lamb, 2020). For the same sediment sizes, larger floods may be needed to initiate debris flows through channel bed failure in higher-order channels because they have lower gradients (e.g., Prancevic et al., 2014). The importance of sediment supply was also discussed by Tang et al. (2019b), who modeled fewer surges associated with debris flow activity through time (going from December 2016 to February 2017), which they attributed to decreased channel sediment supply. Therefore, models that can incorporate both hillslope and channel sediment supply and storm runoff will be beneficial for predicting debris flow hazards in steep and bedrock-dominated landscapes.

CONCLUSIONS

We monitored a burned, steep, first-order catchment within the front range of the San Gabriel Mountains, California, through the course of several storm events in order to make direct observations of debris flow initiation. Following the fire, but prior to the first storm event, most of the hillslope area was stripped to bedrock, and sandy sediment stored behind vegetation dams was transported downhill by dry ravel and accumulated in convergent zones within the catchment, including along the length of the first-order channel network. During a subsequent typical storm event for the region, with peak rainfall intensities of up to 28 mm/hr, runoff was generated in the upper reaches of the catchment, possibly over bedrock outcrops, that led to extensive erosion of the channel fill and failure of the channel bed to produce debris flows and sheetflows. All of the sediment (81.5 m^3) excavated from the channel was deposited in a debris flow fan, allowing us to fully constrain mass balance and show a minimal contribution of hillslope runoff erosion to the total sediment yield.

Our field observations and mass-balance constraints support a "burn-ravel release–channel-bed failure" mechanism for debris flow initiation. Our results are consistent with a vegetation storage and ravel routing model whereby ~30 years of soil production, since the previous wildfire, was transiently stored by vegetation and was transported downslope with a mean granular friction angle of $\tan \bar{\mu} = 0.41$. The model can explain both the volume and location of ravel accumulation in the first order channel by dry processes alone. Our results are also consistent with a channel bed failure model whereby debris flows were initiated in the steep, first order channels that accumulated ravel. The model can explain why a modest, one-year recurrence interval storm event can trigger debris flows, as channel bed failure is more likely to occur in a relatively fine-grained channel bed due to accumulated ravel fill, which causes high Shields numbers that can surpass the threshold for mass failure.

Together, our results suggest that post-fire debris flow initiation and sediment yield in steep, first-order bedrock channels are controlled by dry ravel and in-channel failure. The process transition toward dry ravel and in-channel bed failure is highly sensitive to the fraction of the catchment area that exceeds the angle of dry sediment stability in the absence of vegetation. Rather than hillslope erosion processes, such as rilling and landsliding, that can dominate sediment yield in soil-mantled landscapes and are affected primarily by rainfall intensity and burn severity, debris flow initiation at our site was controlled by sediment supply. Importantly, higher intensity late season storms did not produce debris flows in our catchment because sediment was already stripped from hillsides by dry ravel and evacuated from the channel network following the first moderate storm. Over longer timescales, our results suggest that, unlike soil mantled landscapes, bedrock landscapes subject to increased fire frequency may have reduced sediment yields due to a sediment supply limitation unless fire can significantly affect soil production rates.

ACKNOWLEDGMENTS

We thank Brian Zdeb and Brian Fuller for their help with setting up and collecting field data as well as Jason Kean for useful discussions on debris flow occurrence in the region and for sharing precipitation data from the nearby USGS rain gage. Funding was provided to M.P. Lamb by National Science Foundation grants EAR-1349115 and EAR-1558479 and to M.C. Palucis by National Science Foundation Postdoctoral Fellowship grant EAR-1452337. We thank the reviewers for their time and insightful comments, which helped to improve this manuscript.

REFERENCES CITED

Anderson, H.W., 1949, Flood frequencies and sedimentation from forest watersheds: Eos (Transactions, American Geophysical Union), v. 30, p. 567–586, https://doi.org/10.1029/TR030i004p00567.

Baum, R.L., and Godt, J.W., 2010, Early warning of rainfall-induced shallow landslides and debris flows in the USA: Landslides, v. 7, p. 259–272, https://doi.org/10.1007/s10346-009-0177-0.

Benda, L., and Dunne, T., 1987, Sediment routing by debris flow, *in* Erosion and Sedimentation in the Pacific Rim (Proceedings of the Corvallis Symposium): International Association of Hydrological Sciences Publication 165, p. 213–223, http://hydrologie.org/redbooks/a165/iahs_165_0213.pdf (accessed December 2020).

Berti, M., Genevois, R., Simoni, A., and Tecca, P.R., 1999, Field observations of a debris flow event in the Dolomites: Geomorphology, v. 29, p. 265–274, https://doi.org/10.1016/S0169-555X(99)00018-5.

Berti, M., Genevois, R., LaHusen, R., Simoni, A., and Tecca, P., 2000, Debris flow monitoring in the Acquabona watershed on the Dolomites (Italian Alps): Physics and Chemistry of the Earth, Part B: Hydrology, Oceans and Atmosphere, v. 25, p. 707–715, https://doi.org/10.1016/S1464-1909(00)00090-3.

Burch, G., Moore, I., and Burns, J., 1989, Soil hydrophobic effects on infiltration and catchment runoff: Hydrological Processes, v. 3, p. 211–222, https://doi.org/10.1002/hyp.3360030302.

Cannon, S., Gartner, J., Parrett, C., and Parise, M., 2003, Wildfire-related debris-flow generation through episodic progressive sediment-bulking processes, western USA: Proceedings, Third International Conference on Debris-Flow Hazards Mitigation: Mechanics, Prediction, and Assessment, p. 71–82.

Cannon, S.H., Bigio, E.R., and Mine, E., 2001a, A process for fire-related debris flow initiation, Cerro Grande fire, New Mexico: Hydrological Processes, v. 15, p. 3011–3023, https://doi.org/10.1002/hyp.388.

Cannon, S.H., Kirkham, R.M., and Parise, M., 2001b, Wildfire-related debris-flow initiation processes, Storm King Mountain, Colorado: Geomorphology, v. 39, p. 171–188, https://doi.org/10.1016/S0169-555X(00)00108-2.

Cannon, S.H., Gartner, J.E., Wilson, R.C., Bowers, J.C., and Laber, J.L., 2008, Storm rainfall conditions for floods and debris flows from recently burned areas in southwestern Colorado and southern California: Geomorphology, v. 96, p. 250–269, https://doi.org/10.1016/j.geomorph.2007.03.019.

Cannon, S.H., Gartner, J.E., Rupert, M.G., Michael, J.A., Rea, A.H., and Parrett, C., 2010, Predicting the probability and volume of postwildfire debris flows in the intermountain western United States: Geological Society of America Bulletin, v. 122, p. 127–144, https://doi.org/10.1130/B26459.1.

Cannon, S.H., Boldt, E.M., Laber, J.L., Kean, J.W., and Staley, D.M., 2011, Rainfall intensity—Duration thresholds for postfire debris-flow emergency-response planning: Natural Hazards, v. 59, p. 209–236, https://doi.org/10.1007/s11069-011-9747-2.

Cerdà, A., and Doerr, S.H., 2005, Influence of vegetation recovery on soil hydrology and erodibility following fire: An 11-year investigation: International Journal of Wildland Fire, v. 14, p. 423–437, https://doi.org/10.1071/WF05044.

Certini, G., 2005, Effects of fire on properties of forest soils: A review: Oecologia, v. 143, p. 1–10, https://doi.org/10.1007/s00442-004-1788-8.

Costa, J.E., 1984, Physical geomorphology of debris flows, *in* Costa, J.E., and Fleisher, P.J., eds., Developments and Applications of Geomorphology: Berlin, Heidelberg, Springer, p. 268–317, https://doi.org/10.1007/978-3-642-69759-3_9.

DeLong, S.B., Youberg, A.M., DeLong, W.M., and Murphy, B.P., 2018, Post-wildfire landscape change and erosional processes from repeat terrestrial lidar in a steep headwater catchment, Chiricahua Mountains, Arizona, USA: Geomorphology, v. 300, p. 13–30, https://doi.org/10.1016/j.geomorph.2017.09.028.

Dennison, P.E., Brewer, S.C., Arnold, J.D., and Moritz, M.A., 2014, Large wildfire trends in the western United States, 1984–2011: Geophysical Research Letters, v. 41, p. 2928–2933, https://doi.org/10.1002/2014GL059576.

DiBiase, R.A., 2011, Tectonic Geomorphology of the San Gabriel Mountains, CA [Ph.D. thesis]: Tempe, Arizona State University, 261 p.

DiBiase, R.A., and Lamb, M.P., 2013, Vegetation and wildfire controls on sediment yield in bedrock landscapes: Geophysical Research Letters, v. 40, p. 1093–1097, https://doi.org/10.1002/grl.50277.

DiBiase, R.A., and Lamb, M.P., 2020, Dry sediment loading of headwater channels fuels post-wildfire debris flows in bedrock landscapes: Geology, v. 48, p. 189–193, https://doi.org/10.1130/G46847.1.

DiBiase, R.A., and Whipple, K.X., 2011, The influence of erosion thresholds and runoff variability on the relationships among topography, climate, and erosion rate: Journal of Geophysical Research: Earth Surface, v. 116, no. F4, https://doi.org/10.1029/2011JF002095.

DiBiase, R.A., Whipple, K.X., Heimsath, A.M., and Ouimet, W.B., 2010, Landscape form and millennial erosion rates in the San Gabriel Mountains, CA: Earth and Planetary Science Letters, v. 289, p. 134–144, https://doi.org/10.1016/j.epsl.2009.10.036.

DiBiase, R.A., Lamb, M.P., Ganti, V., and Booth, A.M., 2017, Slope, grain size, and roughness controls on dry sediment transport and storage on steep hillslopes: Journal of Geophysical Research: Earth Surface, v. 122, p. 941–960, https://doi.org/10.1002/2016JF003970.

Dietrich, W.E., Wilson, C.J., and Reneau, S.L., 1986, Hollows, colluvium, and landslides in soil-mantled landscapes, *in* Abrahams, A., ed., Hillslope Processes: Winchester, Allen & Unwin, p. 361–388.

Dingman, S.L., 2015, Physical Hydrology: Long Grove, Illinois, Waveland Press, 658 p.

Dunn, P.H., Barro, S.C., Wells, W.G., Poth, M.A., Wohlgemuth, P.M., and Colver, C.G., 1988, The San Dimas experimental forest: 50 years of research: General Technical Report PSW-104: Berkeley, California, U.S. Department of Agriculture, Pacific Southwest Forest and Range Experiment Station. v. 104, 49 p.

Eaton, E., 1935, Flood and erosion control problems and their solution: American Society of Civil Engineers Transactions, v. 101, p. 1302–1330.

Florsheim, J.L., Keller, E.A., and Best, D.W., 1991, Fluvial sediment transport in response to moderate storm flows following chaparral wildfire, Ventura County, southern California: Geological Society of America Bulletin, v. 103, p. 504–511.

Gabet, E.J., 2003, Sediment transport by dry ravel: Journal of Geophysical Research: Solid Earth, v. 108, no. B1, https://doi.org/10.1029/2001JB001686.

Gabet, E.J., and Bookter, A., 2008, A morphometric analysis of gullies scoured by post-fire progressively bulked debris flows in southwest Montana, USA: Geomorphology, v. 96, p. 298–309, https://doi.org/10.1016/j.geomorph.2007.03.016.

Gabet, E.J., and Mendoza, M.K., 2012, Particle transport over rough hillslope surfaces by dry ravel: Experiments and simulations with implications for nonlocal sediment flux: Particle transport over rough surfaces: Journal of Geophysical Research: Earth Surface, v. 117, no. F01019, https://doi.org/10.1029/2011JF002229.

Gabet, E.J., and Mudd, S.M., 2006, The mobilization of debris flows from shallow landslides: Geomorphology, v. 74, p. 207–218, https://doi.org/10.1016/j.geomorph.2005.08.013.

Gabet, E.J., and Sternberg, P., 2008, The effects of vegetative ash on infiltration capacity, sediment transport, and the generation of progressively bulked debris flows: Geomorphology, v. 101, p. 666–673, https://doi.org/10.1016/j.geomorph.2008.03.005.

Gartner, J.E., Cannon, S.H., Santi, P.M., and Dewolfe, V.G., 2008, Empirical models to predict the volumes of debris flows generated by recently burned basins in the western US: Geomorphology, v. 96, p. 339–354, https://doi.org/10.1016/j.geomorph.2007.02.033.

Gartner, J.E., Cannon, S.H., and Santi, P.M., 2014, Empirical models for predicting volumes of sediment deposited by debris flows and sediment-laden floods in the transverse ranges of southern California: Engineering Geology, v. 176, p. 45–56, https://doi.org/10.1016/j.enggeo.2014.04.008.

Godt, J.W., and Coe, J.A., 2007, Alpine debris flows triggered by a 28 July 1999 thunderstorm in the central Front Range, Colorado: Geomorphology, v. 84, p. 80–97, https://doi.org/10.1016/j.geomorph.2006.07.009.

Guzzetti, F., Peruccacci, S., Rossi, M., and Stark, C.P., 2008, The rainfall intensity–duration control of shallow landslides and debris flows: An update: Landslides, v. 5, p. 3–17, https://doi.org/10.1007/s10346-007-0112-1.

Heimsath, A.M., Dietrich, W.E., Nishiizumi, K., and Finkel, R.C., 1997, The soil production function and landscape equilibrium: Nature, v. 388, p. 358–361, https://doi.org/10.1038/41056.

Heimsath, A.M., DiBiase, R.A., and Whipple, K.X., 2012, Soil production limits and the transition to bedrock-dominated landscapes: Nature Geoscience, v. 5, p. 210–214, https://doi.org/10.1038/ngeo1380.

Hürlimann, M., Rickenmann, D., and Graf, C., 2003, Field and monitoring data of debris-flow events in the Swiss Alps: Canadian Geotechnical Journal, v. 40, p. 161–175, https://doi.org/10.1139/t02-087.

Hyde, K., Woods, S.W., and Donahue, J., 2007, Predicting gully rejuvenation after wildfire using remotely sensed burn severity data: Geomorphology, v. 86, p. 496–511, https://doi.org/10.1016/j.geomorph.2006.10.012.

Inbar, M., Tamir, M., and Wittenberg, L., 1998, Runoff and erosion processes after a forest fire in Mount Carmel, a Mediterranean area: Geomorphology, v. 24, p. 17–33, https://doi.org/10.1016/S0169-555X(97)00098-6.

Iverson, R.M., Reid, M.E., and LaHusen, R.G., 1997, Debris-flow mobilization from landslides 1: Annual Review of Earth and Planetary Sciences, v. 25, p. 85–138, https://doi.org/10.1146/annurev.earth.25.1.85.

Jackson, M., and Roering, J.J., 2009, Post-fire geomorphic response in steep, forested landscapes: Oregon Coast Range, USA: Quaternary Science Reviews, v. 28, p. 1131–1146, https://doi.org/10.1016/j.quascirev.2008.05.003.

Johnson, A., and Rodine, J., 1984, Debris flow, *in* Brunsden, D., and Prior, D.B., eds., Slope Instability: New York, John Wiley, p. 257–361.

Kean, J.W., Staley, D.M., and Cannon, S.H., 2011, In situ measurements of post-fire debris flows in southern California: Comparisons of the timing and magnitude of 24 debris-flow events with rainfall and soil moisture conditions: Journal of Geophysical Research: Earth Surface, v. 116, no. 4, https://doi.org/10.1029/2011JF002005.

Kean, J.W., McCoy, S.W., Tucker, G.E., Staley, D.M., and Coe, J.A., 2013, Runoff-generated debris flows: Observations and modeling of surge initiation, magnitude, and frequency: Journal of Geophysical Research: Earth Surface, v. 118, p. 2190–2207, https://doi.org/10.1002/jgrf.20148.

Keeley, J.E., 1992, Recruitment of seedlings and vegetative sprouts in unburned chaparral: Ecology, v. 73, p. 1194–1208, https://doi.org/10.2307/1940669.

Kotok, E., and Kraebel, C., 1935, Discussion of "Flood and erosion control problems and their solution": Transactions of the American Society of Civil Engineers, v. 101, p. 1350–1355.

Lamb, M.P., Scheingross, J.S., Amidon, W.H., Swanson, E., and Limaye, A., 2011, A model for fire-induced sediment yield by dry ravel in steep landscapes: Journal of Geophysical Research: Earth Surface, v. 116, no. F03006, https://doi.org/10.1029/2010JF001878.

Lamb, M.P., Levina, M., DiBiase, R.A., and Fuller, B.M., 2013, Sediment storage by vegetation in steep bedrock

landscapes: Theory, experiments, and implications for postfire sediment yield: Journal of Geophysical Research: Earth Surface, v. 118, p. 1147–1160, https://doi.org/10.1002/jgrf.20058.

Langhans, C., Nyman, P., Noske, P.J., Van der Sant, R.E., Lane, P.N., and Sheridan, G.J., 2017, Post-fire hillslope debris flows: Evidence of a distinct erosion process: Geomorphology, v. 295, p. 55–75, https://doi.org/10.1016/j.geomorph.2017.06.008.

Lavé, J., and Burbank, D., 2004, Denudation processes and rates in the Transverse Ranges, southern California: Erosional response of a transitional landscape to external and anthropogenic forcing: Journal of Geophysical Research: Earth Surface, v. 109, no. F1.

Lin, J.-W., Chen, C.-W., and Peng, C.-Y., 2012, Potential hazard analysis and risk assessment of debris flow by fuzzy modeling: Natural Hazards, v. 64, p. 273–282, https://doi.org/10.1007/s11069-012-0236-z.

Lindvall, S.C., and Rubin, C.M., 2007, Slip rate studies along the Sierra Madre–Cucamonga fault system using geomorphic and cosmogenic surface exposure age constraints: U.S. Geological Survey Final Technical Report Award Number 03HQGR0084, 13 p.

Los Angeles County Department of Public Works (L.A.C.D.P.W.), 1991, Hydrology Manual: Los Angeles, California, Department of Public Works Hydraulic/Water Conservation Division.

MacDonald, L.H., and Huffman, E.L., 2004, Post-fire soil water repellency: Soil Science Society of America Journal, v. 68, p. 1729–1734, https://doi.org/10.2136/sssaj2004.1729.

Marchi, L., Arattano, M., and Deganutti, A.M., 2002, Ten years of debris-flow monitoring in the Moscardo Torrent (Italian Alps): Geomorphology, v. 46, p. 1–17, https://doi.org/10.1016/S0169-555X(01)00162-3.

Marlon, J.R., et al., 2012, Long-term perspective on wildfires in the western USA: Proceedings of the National Academy of Sciences of the United States of America, v. 109, no. 9, p. E535–E543, https://doi.org/10.1073/pnas.1112839109.

Matti, J.C., and Morton, D.M., 1993, Paleogeographic evolution of the San Andreas fault in southern California: A reconstruction based on a new cross-fault correlation, *in* Matti, J.C., Morton, D.M., and Powell, R., eds., The San Andreas Fault System: Displacement, Palinspastic Reconstruction, and Geologic Evolution: Geological Society of America Memoir 178, p. 107–159, https://doi.org/10.1130/MEM178-p107.

McArdell, B.W., Bartelt, P., and Kowalski, J., 2007, Field observations of basal forces and fluid pore pressure in a debris flow: Geophysical Research Letters, v. 34, no. L07406, https://doi.org/10.1029/2006GL029183.

McCoy, S.W., Kean, J.W., Coe, J.A., Staley, D.M., Wasklewicz, T.A., and Tucker, G.E., 2010, Evolution of a natural debris flow: In situ measurements of flow dynamics, video imagery, and terrestrial laser scanning: Geology, v. 38, p. 735–738, https://doi.org/10.1130/G30928.1.

McGuire, L.A., Rengers, F.K., Kean, J.W., Coe, J.A., Mirus, B.B., Baum, R.L., and Godt, J.W., 2016, Elucidating the role of vegetation in the initiation of rainfall-induced shallow landslides: Insights from an extreme rainfall event in the Colorado Front Range: Geophysical Research Letters, v. 43, p. 9084–9092, https://doi.org/10.1002/2016GL070741.

McGuire, L.A., Rengers, F.K., Kean, J.W., and Staley, D.M., 2017, Debris flow initiation by runoff in a recently burned basin: Is grain-by-grain sediment bulking or en masse failure to blame?: Geophysical Research Letters, v. 44, p. 7310–7319, https://doi.org/10.1002/2017GL074243.

McGuire, L.A., Rengers, F.K., Kean, J.W., Staley, D.M., and Mirus, B.B., 2018, Incorporating spatially heterogeneous infiltration capacity into hydrologic models with applications for simulating post-wildfire debris flow initiation: Hydrological Processes, v. 32, p. 1173–1187, https://doi.org/10.1002/hyp.11458.

Megahan, W.F., King, J.G., and Seyedbagheri, K.A., 1995, Hydrologic and erosional responses of a granitic watershed to helicopter logging and broadcast burning: Forest Science, v. 41, no. 4, p. 777–795.

Mersereau, R., and Dyrness, C., 1972, Accelerated mass wasting after logging and slash burning in western Oregon: Journal of Soil and Water Conservation, v. 27, p. 112–114.

Meyer, G.A., and Wells, S.G., 1997, Fire-related sedimentation events on alluvial fans, Yellowstone National Park, U.S.A: Journal of Sedimentary Research, Section A: Sedimentary Petrology and Processes, v. 67, p. 776-791, http://archives.datapages.com/data/sepm/journals/v66-67/data/067/067005/0776.htm, accessed December 2020.

Meyer, G.A., Pierce, J.L., Wood, S.H., and Jull, A.J.T., 2001, Fire, storms, and erosional events in the Idaho batholith: Hydrological Processes, v. 15, p. 3025–3038, https://doi.org/10.1002/hyp.389.

Miller, J.D., Safford, H., Crimmins, M., and Thode, A.E., 2009, Quantitative evidence for increasing forest fire severity in the Sierra Nevada and southern Cascade Mountains, California and Nevada, USA: Ecosystems, v. 12, p. 16–32, https://doi.org/10.1007/s10021-008-9201-9.

Montgomery, D.R., and Dietrich, W.E., 1989, Source areas, drainage density, and channel initiation: Water Resources Research, v. 25, p. 1907–1918, https://doi.org/10.1029/WR025i008p01907.

Moody, J.A., Shakesby, R.A., Robichaud, P.R., Cannon, S.H., and Martin, D.A., 2013, Current research issues related to post-wildfire runoff and erosion processes: Earth-Science Reviews, v. 122, p. 10–37, https://doi.org/10.1016/j.earscirev.2013.03.004.

Morton, D., 1973, Geology of parts of the Azusa and Mount Wilson quadrangles: San Gabriel Mountains, Los Angeles County, California: California Division of Mines and Geology Special Report, v. 105, 21 p.

Morton, D.M., Miller, F.K., Cossette, P.M., and Bovard, K.R., 2006, Geologic Map of the San Bernardino and Santa Ana 30′ × 60′ Quadrangles, California: U.S. Geological Survey Open-File Report 2006-1217.

Palucis, M.C., Ulizio, T., Fuller, B., and Lamb, M.P., 2018, Intense granular sheetflow in steep streams: Geophysical Research Letters, v. 45, p. 5509-5517, https://doi.org/10.1029/2018GL077526.

Parise, M., and Cannon, S., 2012, Wildfire impacts on the processes that generate debris flows in burned watersheds: Natural Hazards, v. 61, p. 217–227, https://doi.org/10.1007/s11069-011-9769-9.

Parson, A., Robichaud, P.R., Lewis, S.A., Napper, C., and Clark, J.T., 2010, Field guide for mapping post-fire soil burn severity: Gen. Tech. Rep. RMRS-GTR-243: Fort Collins, Colorado, U.S. Department of Agriculture, Forest Service, Rocky Mountain Research Station, v. 243, 49 p.

Pelletier, J.D., and Orem, C.A., 2014, How do sediment yields from post-wildfire debris-laden flows depend on terrain slope, soil burn severity class, and drainage basin area? Insights from airborne-LiDAR change detection: Earth Surface Processes and Landforms, v. 39, no. 13, p. 1822–1832, https://doi.org/10.1002/esp.3570.

Prancevic, J.P., Lamb, M.P., and Fuller, B.M., 2014, Incipient sediment motion across the river to debris-flow transition: Geology, v. 42, p. 191–194, https://doi.org/10.1130/G34927.1.

Prancevic, J.P., Lamb, M.P., Palucis, M.C., and Venditti, J.G., 2018, The role of three-dimensional boundary stresses in limiting the occurrence and size of experimental landslides: Journal of Geophysical Research: Earth Surface, v. 123, p. 46–65, https://doi.org/10.1002/2017JF004410.

Rengers, F.K., McGuire, L.A., Kean, J.W., Staley, D.M., and Hobley, D.E.J., 2016a, Model simulations of flood and debris flow timing in steep catchments after wildfire: Water Resources Research, v. 52, p. 6041–6061, https://doi.org/10.1002/2015WR018176.

Rengers, F.K., Tucker, G., Moody, J., and Ebel, B., 2016b, Illuminating wildfire erosion and deposition patterns with repeat terrestrial lidar: Journal of Geophysical Research: Earth Surface, v. 121, p. 588–608, https://doi.org/10.1002/2015JF003600.

Rengers, F.K., Kean, J.W., Reitman, N.G., Smith, J.B., Coe, J.A., and McGuire, L.A., 2020, The influence of frost weathering on debris flow sediment supply in an Alpine Basin: Journal of Geophysical Research: Earth Surface, v. 125, no. e2019JF005369.

Riley, K.L., Bendick, R., Hyde, K.D., and Gabet, E.J., 2013, Frequency–magnitude distribution of debris flows compiled from global data, and comparison with post-fire debris flows in the western US: Geomorphology, v. 191, p. 118–128, https://doi.org/10.1016/j.geomorph.2013.03.008.

Roering, J.J., and Gerber, M., 2005, Fire and the evolution of steep, soil-mantled landscapes: Geology, v. 33, p. 349–352, https://doi.org/10.1130/G21260.1.

Rowe, P., Countryman, O., and Storey, H., 1954, Hydrologic Analysis Used to Determine Effects of Fire on Peak Discharge and Erosion Rates in Southern California Watersheds: Berkeley, California, U.S. Department of Agriculture, Water Resources Center Archives, University of California, 49 p.

Santi, P.M., Higgins, J.D., Cannon, S.H., Gartner, J.E., et al., 2008, Sources of debris flow material in burned areas: Geomorphology, v. 96, p. 310–321, https://doi.org/10.1016/j.geomorph.2007.02.022.

Scheingross, J.S., and Lamb, M.P., 2016, Sediment transport through self-adjusting, bedrock-walled waterfall plunge pools: Journal of Geophysical Research: Earth Surface, v. 121, p. 939–963, https://doi.org/10.1002/2015JF003620.

Schmidt, K.M., Hanshaw, M., Howle, J.F., Kean, J.W., Staley, D.M., Stock, J.D., and Bawden, G.W., 2011, Hydrologic conditions and terrestrial laser scanning of post-fire debris flows in the San Gabriel Mountains, CA, USA, *in* Proceedings, Fifth International Conference on Debris Flow Hazards Mitigation/Mechanics, Prediction, and Assessment: Padua, Italy, p. 583–593.

Sinclair, J., 1954, Erosion in the San Gabriel Mountains of California: Eos (Transactions, American Geophysical Union), v. 35, p. 264–268, https://doi.org/10.1029/TR035i002p00264.

Singleton, M.P., Thode, A.E., Sánchez Meador, A.J., and Iniguez, J.M., 2019, Increasing trends in high-severity fire in the southwestern USA from 1984 to 2015: Forest Ecology and Management, v. 433, p. 709–719, https://doi.org/10.1016/j.foreco.2018.11.039.

Spittler, T.E., 1995, Fire and the debris flow potential of winter storms, *in* Keeley, J.E., and Scott, T., eds., Brushfires in California Wildlands: Ecology and Resource Management: Fairfield, Washington, International Association of Wildland Fire, p. 113–120.

Spotila, J.A., House, M.A., Blythe, A.E., Niemi, N.A., and Bank, G.C., 2002, Controls on the erosion and geomorphic evolution of the San Bernardino and San Gabriel Mountains, southern California, *in* Barth, A., ed., Contributions to Crustal Evolution of the Southwestern United States: Geological Society of America Special Paper 365, p. 205–230, https://doi.org/10.1130/0-8137-2365-5.205.

Staley, D.M., Wasklewicz, T.A., and Kean, J.W., 2014, Characterizing the primary material sources and dominant erosional processes for post-fire debris-flow initiation in a headwater basin using multi-temporal terrestrial laser scanning data: Geomorphology, v. 214, p. 324–338, https://doi.org/10.1016/j.geomorph.2014.02.015.

Staley, D.M., Negri, J.A., Kean, J.W., Laber, J.L., Tillery, A.C., and Youberg, A.M., 2017, Prediction of spatially explicit rainfall intensity—Duration thresholds for post-fire debris-flow generation in the western United States: Geomorphology, v. 278, p. 149–162, https://doi.org/10.1016/j.geomorph.2016.10.019.

Stock, J., and Dietrich, W.E., 2003, Valley incision by debris flows: Evidence of a topographic signature: Water Resources Research, v. 39, p. 1089, https://doi.org/10.1029/2001WR001057.

Suwa, H., Okano, K., and Kanno, T., 2009, Behavior of debris flows monitored on test slopes of Kamikamihorizawa Creek, Mount Yakedake, Japan: International Journal of Erosion Control Engineering, v. 2, p. 33–45, https://doi.org/10.13101/ijece.2.33.

Suwa, H., Okano, K., and Kanno, T., 2011, Forty years of debris flow monitoring at Kamikamihorizawa Creek, Mount Yakedake, Japan, *in* Proceedings, 5th International Conference on Debris-Flow Hazards Mitigation: Mechanics, Prediction and Assessment: La Sapienza, Roma, Casa Editrice Universita, p. 605–613.

Swanson, F.J., 1981, Fire and geomorphic processes, *in* Mooney, H.A., Bonnicksen, T.M., Christensen, N.L., and Lotan, J.E., technical coordinators, Proceedings, Fire Regimes and Ecosystem Properties Conference. General Technical Report WO-26: Washington,

D.C., U.S. Department of Agriculture, Forest Service, p. 401–444.

Takahashi, T., 1978, Mechanical characteristics of debris flow: Journal of the Hydraulics Division, v. 104, p. 1153–1169.

Tang, H., McGuire, L.A., Rengers, F.K., Kean, J.W., Staley, D.M., and Smith, J.B., 2019a, Developing and testing physically based triggering thresholds for runoff-generated debris flows: Geophysical Research Letters, v. 46, p. 8830–8839, https://doi.org/10.1029/2019GL083623.

Tang, H., McGuire, L.A., Rengers, F.K., Kean, J.W., Staley, D.M., and Smith, J.B., 2019b, Evolution of debris-flow initiation mechanisms and sediment sources during a sequence of post-wildfire rainstorms: Journal of Geophysical Research: Earth Surface, v. 124, p. 1572-1595, https://doi.org/10.1029/2018JF004837.

Tarboton, D.G., 1997, A new method for the determination of flow directions and upslope areas in grid digital elevation models: Water Resources Research, v. 33, p. 309–319, https://doi.org/10.1029/96WR03137.

Tillery, A.C., and Rengers, F.K., 2020, Controls on debris-flow initiation on burned and unburned hillslopes during an exceptional rainstorm in southern New Mexico, USA: Earth Surface Processes and Landforms, v. 45, p. 1051–1066, https://doi.org/10.1002/esp.4761.

Tucker, G.E., and Bradley, D.N., 2010, Trouble with diffusion: Reassessing hillslope erosion laws with a particle-based model: Journal of Geophysical Research: Earth Surface, v. 115, no. F00A10, https://doi.org/10.1029/2009JF001264.

Wells, W.G., II, 1982, The storms of 1978 and 1980 and their effect on sediment movement in the eastern San Gabriel front, *in* Storms, Floods, and Debris Flows in Southern California and Arizona 1978 and 1980: Overview and Summary of a Symposium, September 17–18, 1980, Pasadena, California: Washington, D.C., National Academy Press, National Academy of Sciences, National Research Council Rep. No. CSS-CND-019, 229 p.

Wells, W.G., 1987, The effects of fire on the generation of debris flows in southern California, *in* Costa, J.E., and Wieczorek, G.F., Debris Flows/Avalanches: Boulder, Colorado, Geological Society of America, Reviews in Engineering Geology, v. 7, p. 105–114, https://doi.org/10.1130/REG7-p105.

Wells, S.G., McFadden, L.D., and Dohrenwend, J.C., 1987, Influence of late Quaternary climatic changes on geomorphic and pedogenic processes on a desert piedmont, eastern Mojave Desert, California: Quaternary Research, v. 27, p. 130–146, https://doi.org/10.1016/0033-5894(87)90072-X.

Wondzell, S.M., and King, J.G., 2003, Postfire erosional processes in the Pacific Northwest and Rocky Mountain regions: Forest Ecology and Management, v. 178, p. 75–87, https://doi.org/10.1016/S0378-1127(03)00054-9.

Woods, S.W., and Balfour, V.N., 2010, The effects of soil texture and ash thickness on the post-fire hydrological response from ash-covered soils: Journal of Hydrology, v. 393, p. 274–286, https://doi.org/10.1016/j.jhydrol.2010.08.025.

Science Editor: Brad S. Singer
Associate Editor: Karl Wegmann

Manuscript Received 8 July 2020
Revised Manuscript Received 3 December 2020
Manuscript Accepted 16 December 2020

Printed in the USA